HIF1α stability in hypoxia is not oxidant-initiated but can be tuned by redox regulation of the proteasome

Amit Kumar[1, 2, 3], Manisha Vaish[1, 4], Saravanan S. Karuppagounder[1, 2, 3], Irina Gazaryan[5], John W. Cave[1, 2, 3], Anatoly A. Starkov[2, 3], Elizabeth T. Anderson[6], Sheng Zhang[6], John T. Pinto[7], Austin Rountree[8], Wang Wang[9], Ian R. Sweet[8] and Rajiv R. Ratan[1, 2, 3, *]

[1]Burke Neurological Institute, White Plains, NY, 10605, USA
[2]Brain and Mind Research Institute and [3]Department of Neurology, Weill Medical College of Cornell University, New York, 10016, USA
[4]Department of Pharmacological Sciences, Icahn School of Medicine at Mount Sinai, New York, 10029, USA
[5]Department of Anatomy and Cell Biology, New York Medical College, Valhalla, NY, 10595, USA
[6]Institute for Biotechnology, Cornell University, Ithaca, NY, 14853, USA
[7]Department of Biochemistry and Molecular Biology, New York Medical College, Valhalla, NY, 10595, USA
[8]Department of Medicine, University of Washington, Seattle, WA, 98108, USA
[9]Department of Pain and Anesthesiology, University of Washington, Seattle, WA, 98195, USA

Correspondence should be addressed to:

[*]Rajiv R. Ratan M.D., Ph.D.
Burke Neurological Institute at Weill Cornell Medicine
785 Mamaroneck Avenue
White Plains, NY, 10605, USA
Email: rrr2001@med.cornell.edu
Phone: 914-597-2225

Abstract

Hypoxic adaptation mediated by HIF transcription factors requires mitochondria, which can increase peroxide to regulate HIF1α stability in hypoxia. Here, we use state-of-the-art tools to evaluate the role of peroxide and other reactive oxygen species (ROS) in regulating HIF1α stability. We show that antioxidant enzymes are neither homeostatically induced nor are peroxide levels increased in hypoxia. Forced expression of diverse antioxidant enzymes, all of which diminish peroxide, had disparate effects on HIF1α protein stability. Reduction of lipid peroxides by glutathione peroxidase-4 or superoxide by mitochondrial SOD, failed to influence HIF1α protein stability. These data showed that mitochondrial, cytosolic or lipid ROS were not necessary for HIF1α stability. In contrast, altering the cellular redox state to favor oxidized glutathione (GSSG) enhanced HIF1α stability via enhanced and selective *S*-glutathionlylation of proteasomal subunits. These data suggest that hypoxia-specific signals that drive HIF-1α stability can be tuned by redox regulation of the proteasome.

Keywords

Hypoxia, Mitochondria, Peroxide, Reactive oxygen species, HIF1α stability, *S*-glutathionylation, VHL, HIF PHDs, Oxygen, Ischemia, Cancer, Stroke

Introduction

Over the past decade, our ability to monitor and manipulate reactive oxygen species (ROS) has grown enormously. These technological advances provide a novel view on how ROS interact with cells to modulate function. Specifically, ROS such as peroxide can act as cellular messengers. Messenger functions for ROS reflect their tight spatial control within cells. The tight spatial control of ROS has enabled their critical roles in growth factor signaling, inflammation, and regeneration (1-3). Specific signaling roles for ROS are facilitated by the existence of motifs in proteins such as phosphatases that render these proteins specifically susceptible to redox modulation (4-6).

An important area of biology where ROS signaling has been highly investigated but where no consensus has emerged is hypoxic adaptation. Seminal work from Semenza, Kaelin and Ratcliffe demonstrated that when oxygen tension falls below a critical threshold, that a family of enzymes dependent on oxygen, iron and 2-oxoglutarate known as the HIF Prolyl Hydroxylases (HIF PHDs) reduce their activity, leading to diminished hydroxylation of the alpha subunit of HIF transcription factors (7-14). Diminished HIF1α hydroxylation reduces recruitment of a key E3 Ubiquitin ligase, the von Hippel Lindau (VHL) protein, which allows HIF1α to avoid proteasomal degradation. Stabilized HIF1α dimerizes with its constitutively active partner to bind to hypoxia response elements in a coordinate gene cassette that leads to hypoxic adaptation at a cellular, local and systemic level (9, 15, 16). HIF transcription factors have been implicated in limiting damage to the kidney, heart and brain, and in progression of a host of cancers as well as pulmonary fibrosis. So, understanding the role of ROS in HIF1α mediated adaptation has numerous clinical implications (17-22).

Previous studies have shown that the dose response of HIF1α stability to progressively lower oxygen concentrations required other factors besides oxygen to regulate HIF PHD activity (23-26). Using then state of the art tools to monitor ROS, it was shown that during hypoxia ROS were increasing and that pharmacological tools that nullified this increase in ROS diminished HIF1α stability (23). A compelling model emerged that hypoxia increases the flux of electrons via Rieske Iron Sulfur cluster proteins in complex III and this leads to an increase in mitochondrial ROS generation via the ubiquinone binding site near the outer leaflet of the inner mitochondrial membrane (the Qo site) (26). Peroxide generated at this site could then diffuse through the outer mitochondrial membrane to inhibit HIF PHDs via either direct redox modulation of HIF PHDs (26) or activation of established redox sensitive p38 MAP kinase signaling (27).

Since its inception, the role of mitochondria established by Chandel and Schumacker in HIF signaling has been validated (25, 28, 29). However, an alternate ROS-independent view of how mitochondria regulate HIF1α stability in hypoxia has also been advanced. Pharmacological inhibition of ETC complexes or genetic knockdown of Rieske Fe/S proteins or cytochrome c not only inhibits mitochondrial ROS production (23-26), it also inhibits oxygen consumption. In this distinct scheme, inhibition of ETC function would alter the kinetics of reduction of cytosolic oxygen levels. Indeed, several groups have provided data supporting the importance of respiratory chain driven mitochondrial oxygen consumption in dictating cellular oxygen gradients. These gradients have been hypothesized to reduce oxygen concentrations to levels required to inhibit enzymatic activity of oxygen dependent HIF PHDs-the key upstream regulator of HIF1α stability (30-32).

In this manuscript, we leverage a host of complementary approaches that support the conclusion that peroxide is a dispensable mediator of regulated HIF1α stability in hypoxia.

Unexpectedly, our results suggest that while HIF1α stability in hypoxia is not oxidant-initiated, that the changes in the cellular redox state imposed by pharmacological agents during hypoxia provide a mechanism for gain modulation of HIF1α stability via post-translational inhibition of proteasomal subunits.

Results

Antioxidant enzymes are not homeostatically induced in hypoxia

Increases in ROS that are sufficient for signaling or toxicity trigger homeostatic transcriptional increases in antioxidant enzymes (33). To assess whether hypoxia results in similar homeostatic increases in antioxidant protein expression, we exposed human neuroblastoma (SH-SY5Y) cells to hypoxia for 8 hours and measured protein expression levels of peroxisomal, cytosolic and mitochondrial antioxidant enzymes including catalase, glutathione peroxidase-1 (GPX1), glutathione peroxidase-4 (GPX4), MnSOD, and Peroxiredoxin-3 (PRDX3) (Figure 1A). The 8 hour time point was chosen to monitor homeostatic changes in antioxidant enzymes because this would be 6 hours following observable HIF1α stability in hypoxia in SH-SY5Y cells, which provides adequate time for homeostatic increases to initiate transcriptional or post-transcriptional adaptations. At the 8 hour time point, the protein level of the peroxisomal antioxidant catalase, and antioxidants present in both cytosol and mitochondria, such as GPX1 and GPX4, showed no change in hypoxia with normalization to Actin (Figures 1B and 1C). However, since hypoxia induces HIF1α-dependent mitophagy (34, 35), mitochondrial mass is decreased with increasing duration of hypoxia, including decreases in mitochondrial DNA and proteins. Accordingly, we normalized distinct mitochondrially-targeted antioxidant enzymes to the level of citrate synthase, a mitochondrial protein. When normalized to citrate synthase, the

expression levels of mitochondrial antioxidants, such as MnSOD and PRDX3, also did not change in hypoxia (Figures 1D and 1E). To establish whether these findings apply to non-transformed cells, we studied expression levels of antioxidant enzymes in hypoxia in primary neurons. Similar to neuroblastoma cells, antioxidant enzyme levels did not change in hypoxia in post-mitotic neurons (Figures 1F-1I). Together, these findings suggest that ROS levels do not increase during hypoxia.

Peroxide levels do not increase during hypoxia

HyPer is a fusion protein composed of the peroxide-sensitive domain of the prokaryotic transcription factor, OxyR, and yellow fluorescent protein that is a reporter for cellular peroxide (36). This reporter is not only sensitive and specific, but its activity is also ratiometric, which factors out differences in fluorescence due to cell geometry, path length, and reporter concentration. Prior studies showed that enhanced pH buffering of the extracellular medium alleviates the putative effects of acidic pH during hypoxia on the reporter, and that fluorescent ratios can be calibrated in cells to known peroxide concentrations (37).

To monitor changes in the level of hydrogen peroxide (H_2O_2), we used real-time imaging of rat pancreatic islet cells in hypoxia with strong pH buffering. Pancreatic islet cells, rather than neurons or neuron-like cells, were used for initial analysis because mitochondrial peroxide in pancreatic islet cells increases in response in extracellular glucose levels, as measured using HyPer imaging. Elevated glucose, therefore, can be used as a positive control for mitochondrial peroxide increases. Additionally, elevated glucose increases insulin release in beta islet cells, which enables insulin release assays to establish cell viability if there is an absence of peroxide changes during hypoxia. Similar real-time measures of cell function are not readily available in primary neurons or SH-SY5Y neuroblastoma cells. Prior studies have also established that

glucose-induced peroxide formation is derived from the mitochondria. Specifically, increased expression of mitochondrial catalase reduced glucose-induced HyPer signals (catalase scavenges peroxide), as did reduced expression of mitochondrial SOD (MnSOD; the enzyme that converts superoxide to peroxide) (37). Finally, signaling levels of peroxide measured by HyPer are 1/20th those of peroxide levels required for toxicity (37), which demonstrates the sensitivity of peroxide measurements using HyPer in this cell type. Before assaying peroxide in hypoxia, we verified that two hours of hypoxia induced the established HIF1α target genes *Kdm6b* and *Bnip3* in islet cells in our flow culture system (Figures 1J and 1K) (38). This time point was selected to evaluate the role of peroxide in mediating the earliest changes in HIF1α stability in hypoxia because it is well before mitochondrial autophagy is induced (Figure 1).

Accordingly, based on the sensitivity and specificity of the reporter assay, we were confident that mitochondrial peroxide was measureable in islet cells if it were increased in hypoxia. H_2O_2, NAD(P)H, and insulin secretion rates were measured simultaneously as a function of glucose concentration for two hours under hypoxic conditions (1% O_2) (Figure 1L). Increasing glucose concentration from 3 mM to 20 mM elicited expected increases in peroxide, decreases in NADPH levels, and insulin secretion rates under normoxia. When islet cells under the same glucose concentrations (20 mM) were exposed to 1% oxygen, H_2O_2 decreased by more than 80%. This reduction occurred in the midst of increased NAD(P)H levels. NADP(H) likely increased due to diminished utilization by the mitochondrial electron transport chain. Glucose-stimulated insulin secretion decreased by about 50% in response to hypoxia, but remained well above unstimulated rates, indicating that islets remained functional throughout the study. Indeed, restoring steady state O_2 levels (20%) resulted in expected increases in

peroxide and insulin secretion with concomitant decreases in NAD(P)H, which indicates hypoxia delivered under the conditions of our experiments is not toxic to islet cells (Figure 1L).

To establish the generalizability of these findings to other cell types, we measured HyPer reporter fluorescence ratios in hypoxic in SH-SY5Y and Hep3B human hepatocellular carcinoma cells. Ratiometric imaging of both cell types showed no change in peroxide levels following two hours of hypoxia, which was sufficient time to activate HIF1α -dependent gene expression. This absence of changes in peroxide levels during hypoxia could not be attributed to a lack of HyPer reporter responsiveness to peroxide in these cell types since complex IV inhibition (KCN) (Figure S1C) or exogenous addition of peroxide (Figure S1G) following the hypoxic exposure led to expected, significant increases in reporter activity. Together with our antioxidant protein expression results, these data suggest that mitochondrial peroxide either decreases or is unchanged by hypoxia in primary (pancreatic beta islets) and transformed cell types (SH-SY5Y, Hep3B), respectively.

HIF1α stabilization is not oxidant-initiated in hypoxia

In order to study directly the regulation of HIF1α protein stabilization in hypoxia, we established the sensitivity and dynamic range of HIF-luciferase reporter protein levels. The HIF-luciferase reporter contains the oxygen dependent domain (ODD) of HIF1α fused to luciferase (ODD-luciferase). Prior studies from one of our groups have demonstrated that this reporter behaves like endogenous HIF but does not influence endogenous HIF activity (39, 40). After treatment with deferoxamine (DFO), a canonical HIF PHD inhibitor, we found that HIF reporter protein levels could be monitored dynamically across a wide range of DFO concentrations (Figure 2A and 2B). As an independent measure, we also assayed the activity of HIF1α-luciferase reporter by measuring luciferase activity. These assays showed that the HIF1α-

luciferase reporter measured by photometric luciferase activity possesses a high dynamic range and low coefficient of variation (Figure 2C). Indeed, changes in HIF1α-luciferase activity measurements with increasing doses of DFO showed a strong correlation with quantitative changes in HIF1α-luciferase reporter protein levels measured by quantitative immunoblotting (Figure 2D).

Prior studies showed that decreasing ROS by forced expression of individual antioxidant enzymes can decrease HIF1α protein levels (23, 24). To confirm these findings with our HIF1α-luciferase reporter, we forced expression of either catalase (a peroxide scavenger), GPX1 (a peroxide scavenger), or MnSOD (a superoxide scavenger and peroxide generator) (Figure 2E). SH-SY5Y cells expressing ODD-Luc were transduced with individual antioxidant enzymes encoded in distinct adenoviral constructs or an adenovirus encoding GFP only as a protein control. Seventy-two hours following infection, GFP expression was observed in nearly 90% of SH-SY5Y cells (Figures S2A and S2B). Accordingly, cells were tested for specific enzyme activities of MnSOD, Catalase, or GPX1. These studies showed a seven-, eleven-, and three-fold increase in specific activity over GFP controls for MnSOD-, Catalase-, and GPX1-expressing cells, respectively (Figures 2F, 2G and 2H).

Having verified increases in individual antioxidant enzyme activities (MnSOD, GPX1, and Catalase) that can either increase (MnSOD) or decrease peroxide (GPX1, Catalase), we examined the effect of these manipulations on HIF1α stability. The mitochondrial peroxide model of HIF regulation predicts that MnSOD should increase HIF1α stability in hypoxia, whereas GPX1 and catalase should diminish HIF1α stability. In contrast to these predictions, we found that MnSOD had no effect on HIF1α reporter activity, while Catalase increased reporter activity, and GPX1 decreased it (Figure 3A). To verify that our HIF1α luciferase reporter accurately

reflected endogenous HIF1α levels, we performed quantitative fluorescence immunoblotting. These assays showed changes in endogenous HIF1α protein are similar to those identified with the HIF1α reporter (Figure 3B). From these findings, we conclude that HIF1α levels are not correlated with mitochondrial peroxide production. Since catalase is a peroxisomal enzyme and GPX1 localizes to the cytosol and mitochondria, our results could not formally exclude the possibility that GPX1 localization to the mitochondria allowed it to reduce HIF1α levels, while Catalase's inability to penetrate this compartment did not allow it to reduce HIF1α levels. To address this possibility, we forced expression of PRDX3, a member of the peroxiredoxin family of antioxidant enzymes that functions as a thioredoxin-dependent peroxide reductase in the mitochondria. Contrary to GPX1, PRDX3 increased levels of HIF1α in hypoxia as measured by either HIF1α reporter activity (Figure 3C) or quantitative fluorescence immunoblotting (Figure 3D). We also confirmed these findings in primary neurons (Figures 3E and 3F), where adenoviral constructs also effectively increased expression of the antioxidant enzymes (Figures S2C and S2D). As a final test of whether GPX1, PRDX3, or catalase reduce oxidant production in SH-SY5Y cells, we measured 5, 6 carboxydichlorofluorescein fluorescence (a non-selective redox sensitive reporter) using flow cytometry. These experiments confirmed the ability of GPX1, PRDX3, and catalase to reduce steady state DCF oxidation, presumably resulting from oxidants generated physiologically (Figures S3A and S3B). However, there was no significant change in peroxide level in response to MnSOD expression despite a significant increase in the MnSOD enzyme activity and protein level. This was unexpected and could reflect compensatory activation of other antioxidants such as GPX1, GPX4 or Prdx3 in response to increased MnSOD activity. We verified that DCF loading and corresponding antioxidant effects were not different

from normoxic or hypoxic cells, arguing against the possibility that our redox reporter or the antioxidant enzymes are behaving differently in normoxia and hypoxia (Figures S3D and S3E).

Our findings did not exclude the possibility that antioxidants alter HIF1α protein levels by differentially regulating either *Hif* mRNA synthesis or *Hif* mRNA stability. Accordingly, we monitored *Hif1α* mRNA levels in the cells overexpressing Catalase, GPX1, and PRDX3. Quantitative PCR revealed that *Hif* mRNA levels were not changed in a manner that would contradict the observed ROS-independent changes in HIF1α stability (Figures 4A and 4B). To confirm that changes observed in HIF1α protein stability are related to changes in its half-life, we examined the stability of HIF1α protein in the presence of cycloheximide, which suppresses de novo protein synthesis in cells pre-treated either with or without MG132. As expected, we found that Catalase and PRDX3, which increase HIF1α protein levels, also increased HIF1α half-life (Figures 4C, 4D and 4E). By contrast, GPX1, which diminished HIF1α protein levels, decreased HIF1α half-life (Figure 4D). Moreover, MG132 treatment significantly enhanced Hif-1α half-life in all cases showing that the antioxidant led changes in hypoxic Hif-1α stabilization were the results of alterations in proteasomal degradation.

To establish whether our findings in primary neurons and neuroblastoma cells can be extended to non-neural cell types, we examined the ability of antioxidant enzymes capable of modulating peroxide levels to modulate HIF1α stability in hypoxic Hep3B hepatocarcinoma cells and hypoxic HeLa cervical cancer cells. Forced expression of Catalase, GPX1, or PRDX3 using adenoviral vectors significantly increased in protein levels of each of the antioxidant enzymes in Hep3B or HeLa cells (Figures S4 and S5). Similar to primary neurons or neuroblastoma cells, we did not observe a uniform reduction in HIF1α stability in hypoxia by enzymes whose common activity is

to reduce peroxide in these non-neural cell types (Figures S4 and S5). Altogether, our findings suggest that peroxide levels are uncoupled from HIF1α stability in neural and non-neural cells.

Is Factor Inhibiting HIF a target for ROS in hypoxia?

Previous studies have highlighted the role that Factor Inhibiting HIF (FIH) in the redox regulation of HIF1α. FIH inhibits HIF-dependent transcription by hydroxylating an asparagine in the C-terminal domain of the HIF1α protein that can interact with the co-activator, CBP in hypoxia (41-43). Suppression of FIH should, therefore, facilitate CBP recruitment and enhance HIF1α target gene transcription. To determine whether a change in HIF-dependent transcription correlated with changes in HIF1α protein levels, we examined *Enolase2* and *Bnip3* mRNA expression levels, which are two established HIF1α target genes (44, 45)) in neuroblastoma SH-SY5Y cells and primary cortical neurons (PCNs). As expected, changes in *Enolase2* and *Bnip3* mRNA levels correlated with HIF1α luciferase reporter levels (Figures 5A-5F). These results suggest that the differential regulation derives from differential effects of antioxidant enzymes on HIF1α protein stability not on FIH.

Neither Reactive Oxygen Species nor Reactive Lipid Species regulate HIF-1α stability in hypoxia

Recent compelling evidence showed that reactive lipid species (RLS) are sufficient to drive HIF-dependent transcription via their effects on FIH inhibition without affecting HIF1α stability (46). Accordingly, we forced expression of GPX4, a selenoprotein that neutralizes RLS (Figure 6A). To manipulate steady-state levels, we used GPX4 protein fused to an optimized destabilization domain (dd) from the prokaryotic dihydrofolate reductase gene. The dd domain destabilizes GPX4 protein unless trimethoprim (TMP, 10 μM) is present (Figure 6B). TMP enhanced GPX4 levels in neuroblastoma cells expressing ddGPX4, but increasing GPX4 levels

had no effect on hypoxia-induced HIF1α stability (Figures 6C-6D) or HIF1α-dependent transcription (Figures 6E and 6F). We verified that GPX4 diminished RLS (Figure S3C) and neutralized ferroptosis induced by glutamate, a form of cell death mediated by reactive lipid species that is abrogated by GPX4 (Figures 6G and 6H) (47). Altogether, these findings argue against a central role for hydrogen peroxide or lipid peroxides in mediating HIF1α stabilization in hypoxia.

Stabilization of HIF1α is redox-modulated in hypoxia: a strategy for therapeutic manipulation of the adaptive hypoxic response

Since we could not substantiate that HIF1α stability was oxidant-initiated in hypoxia, we considered the possibility that HIF1α can be redox-regulated in the absence of increases in ROS. Glutathione has a molecular weight of 307.3 daltons and when covalently attached to cysteinyl residues can alter the charge of its client protein and thus alter function. Previous studies showed that HIF-1α can be S-glutathionylated under hypoxic or normoxic conditions in the presence of oxidizing agents (e,g, GSSG-methyl ester, AAP) (48). Under this scheme, increases in GSSG could be used to stabilize HIF1α in hypoxia. In keeping with this model and prior published studies, we found that BCNU (1,3-bis-(2-chloroethyl)-1-nitrosourea), a chemotherapeutic agent known to inhibit GR and to increase the GSSG/GSH ratio, enhanced ODD-luciferase activity in hypoxia. Similarly, other agents that increase the GSSG/GSH ratio, such as diamide (an oxidizing sulfhydryl agent) or GSSG methyl ester (a cell permeant form of GSSG), also increased HIF1α levels in hypoxia as compared to vehicle control (Figure 7A). By contrast, GSH ethyl ester, a cell permeant form of reduced glutathione expected to decrease the GSSG/GSH ratio, significantly reduced HIF1α reporter stability in hypoxia. Similarly, NAC, which can also decrease the ratio of GSSG/GSH, diminished HIF1α reporter levels in hypoxia (Figure 7A). Furthermore,

we confirmed the functional capacity of BCNU and GSHEE to modulate global glutathionylation (Figure 7B).

These findings agree with previous studies showing that the cellular redox state tunes the level of HIF1α under hypoxia. Changes in oxidized glutathione are able to modulate HIF signaling via *S*-glutathionylation of target cysteines (49, 50). To directly test the role of *S*-glutathionylation in hypoxia signaling, we forced expression of GRX1, which removes glutathione adducts from cysteines in proteins. As expected from our pharmacological data, GRX1 significantly decreased ODD-luciferase activity and protein levels of ODD-luciferase and HIF1α protein (Figures 7C and 7D). Forced expression of GRX1 also had no effect on *Hif1α* message levels (Figure 7E), which was consistent with a role in decreasing HIF1α protein stability. Accordingly, we found that GRX1 not only reduced hypoxia-induced HIF1α protein levels, but also reduced expression of *Enolase2* and *Bnip3*, the established HIF1α-regulated genes (Figures 7F and 7G). Together, these findings demonstrate that agents known to increase protein S-glutathionlylation (e.g., BCNU, diamide, GSSG methyl ester) positively regulate HIF1α stability, while reducing protein *S*-glutathionylation (GSHEE, NAC and GRX1 overexpression) reduces HIF1α stability. Of note, glutathione adducts of cysteine residue 520 (C520) in the oxygen degradation domain (ODD) of human HIF1α were recently shown to play a key role in regulating the stabilization of HIF1α under ischemia (51). We created a cysteine-to-serine (C520S) mutant HIF1α protein and found that this mutated protein did not block the increase in stabilization of HIF1α in hypoxia or ischemia (modelled by in-vitro oxygen-glucose deprivation [OGD] in cultured neurons in dishes), which was contrary to the recent report (Figure 7H). Since there are no other cysteines in the ODD domain, these results suggest that another regulator of HIF1α stability (e.g. HIF PHDs or VHL) is the target for changes in the cellular redox state and

consequent *S*-glutathionylation (Figure 7H). In this scheme, *S*-glutathionylation may be the end product of conversion of susceptible sulfhydryl moieties of cysteines in a modulator of HIF1α stability to that of an oxidized sulfenyl moiety.

To explore this possibility further, we performed a proteomic assessment of proteins that undergo significant *S*-glutathionylation in hypoxia. We used genetic as well as pharmacological approaches. The genetic approach included the overexpression of GRX1, which decreases the protein S-glutathionylation. In pharmacological approach, we treated cells with either BCNU, an agent that increases protein S-glutathionylation and this served as positive control or GSHEE, an agent that decreases protein S-glutathionylation and this served as negative control (Figure 8A). Consistent with our mutant HIF1α reporter studies (Figure 7H), we did not observe a significant increases in HIF1α *S*-glutathionylation (Figure 8B). Unexpectedly, we also did not find increases in *S*-glutathionylation of proteins that are involved in modulating HIF1α stability, including all three HIF PHD isoforms, the E3 ubiquitin ligase, VHL, and Siah proteins (which are known to regulate HIF PHD stability) (Figures 8B). Importantly, we cannot exclude the formal possibility that our redox proteomics is not sufficiently sensitive to detect glutathionylation of pathway specific HIF-1 regulators.

Interestingly, we found congruent changes specifically under hypoxia in *S*-glutathionylation of RPN1 and RPN2 (two proteasomal subunits involved in indirect binding of substrates to the proteasome) according to changes in glutathionylation status of cells induced by pharmacological and genetic means (Figure 8C; Figures S6-S8; Figure 8A). Notably, changes in HIF1α reporter activity (ODD-luciferase activity) were highly correlated with changes in *S*-glutathionylation of RPN1 and RPN2 (Figures 8D and 8E). This led us to explore the possibility that proteasomal activity is directly reduced under hypoxia to facilitate HIF1α stability. In fact,

we did find decrease in proteasomal activity in SH-SY5Y cells as well as primary neurons (Figures 8F and 8G).

Proteasomal degradation of substrates occurs via two independent pathways that involve either direct binding of poly-ubiquitin side chains or indirect binding via bivalent shuttles to the 19S regulatory particle, which is composed of a lid and a base. At the base of the 19S regulatory particle, substrates undergo deubiquitination and unfolding in preparation for degradation in the 20S core particle. RPN1 and RPN2 bind bivalent shuttles of substrates at the base of the 19S regulatory particle, and inhibition of RPN1 or RPN2 function would be expected to diminish 26S proteasomal activity. Indeed, prior studies demonstrated that *S*-glutathionylation of RPN1 and RPN2 in response to exogenously added peroxide diminishes cellular proteasomal activity (52). Inhibition of proteasomal activity mediated via glutathionylation of RPN1 or RPN2 in hypoxia would be expected to modulate the gain of HIF1α stability driven by more specific hypoxia-mediated inhibition of HIF PHD activity. Accordingly, we found that under hypoxia, enhancing protein *S*-glutathionylation with BCNU increased proteasomal activity while decreasing protein S-glutathionylation with either GSHEE or forced expression of GRX1 reduced proteasomal activity significantly and specifically in hypoxia (Figure 8H).

Proteasome substrates are recognized by poly-ubiquitin receptors, Rpn10 and Rpn13. The scaffolding proteins, Rpn1 and Rpn2 serve as docking sites for these ubiquitin receptors. Rpn10 attaches to the central portion of Rpn1 and this association is stabilized by Rpn2 while Rpn13 binds directly to the Rpn2. We hypothesized that *S*-glutathionylation of Rpn1 and Rpn2 might affect the docking of ubiquitin receptors, Rpn10 and Rpn13. Accordingly, we found that hypoxia decreased the interaction of Rpn13 with ubiquitin (Figure 9A), but simultaneously enhanced the interaction of Rpn13 with Rpn2 (Figure 9C). These findings are consistent with *S*-

glutathionylation of Rpn2 increasing the stability of ubiquitinated HIF-1α by sequestering Rpn13. Similarly, we found decrease in Rpn10-Ubiquitin interaction (Figure 9B). Moreover, we also found that hypoxia significantly diminished the interaction of Rpn10 with Rpn1 and Rpn2 (Figures 9D and 9E). These data suggest that Rpn10, which is held tightly by Rpn1 and Rpn2 under normoxia in order to facilitate its interaction with ubiquitin, is functionally compromised by hypoxia and reduces its interaction with Rpn1 and Rpn2. Altogether, these data demonstrate that hypoxia decreases the binding affinity of proteasomal substrates with ubiquitin receptors, Rpn10 and Rpn13 by impacting their interaction with docking proteins, Rpn1 and Rpn2. Moreover, these findings are consistent with the notion that glutathione adduction by Rpn1 or Rpn2 modifies interactions among ubiquitinated proteins and the proteasome in the indirect pathway (Figure 9F).

Discussion

Seminal studies have supported the notion that mitochondria are essential regulators of hypoxic adaptation possibly acting via their ability to generate peroxide (28, 53). In this paper, we show that HIF1α stability mediated by HIF PHDs during hypoxia does not require peroxide. These data include our inability to detect an increase in peroxide during hypoxia (Figure 1L); the lack of homeostatic changes in antioxidant protein expression during hypoxia (Figures 1B-1I); and the failure of forced expression of antioxidant enzymes (Catalase, GPX1, and PRDX3) with the common ability to diminish cellular peroxide to influence HIF1α stability and transcription in the same direction (Figures 3 and 5). Our findings agree with prior studies that showed: 1) that HIF PHDs are not inhibited by exogenously added peroxide (32), and 2) that forced expression of an alternative oxidase which directly transfers electrons from coenzyme Q to oxygen to form

water maintains HIF1α stability in hypoxia, despite reducing superoxide generation at Complex III (32). Our results cannot be attributed to differences in mitochondrial ROS generation by transformed versus primary cells, or to differences in neuron-like versus non-neural cells, as SH-SY5Y neuroblastoma cells and primary cortical neurons showed similar effects, as did Hep3B hepatocellular carcinoma cells and HeLa cervical cancer cells. While we cannot exclude the possibility that culture conditions such as serum lots could reconcile our results with prior studies, in aggregate, the findings favor a role for mitochondria in modulating HIF1α stability via their effects as oxygen consumers not as peroxide second messenger generators.

Peroxide scavengers have distinct effects on hypoxic HIF1α stability

Prior studies have shown that in some cell types, ROS generation in hypoxia could be related to increased oxidant production or decreased defenses (54). In order to address that the imbalance of oxidants and antioxidants plays the regulatory role in mediating hypoxia signaling, we forced expression of distinct antioxidant enzymes known to either reduce (GPX1, Catalase, and PRDX3) or enhance peroxide levels (MnSOD). Despite evidence for increased activity of the antioxidant enzymes studied using multiple experimental approaches, we found that HIF1α stability and transcription did not correlate with effects on peroxide levels. Indeed, MnSOD had no effect on HIF1α stability, GPX1 diminished HIF1α stability, and catalase and PRDX3 increased HIF1α stability in neuroblastoma cells and primary neurons (Figures 3A-3D). Similar uncoupling was observed in non-neural cell types as well (Figures S4 and S5). The results uncouple peroxide generation in the mitochondria from HIF1α stability via the HIF PHDs. It is likely that the GPX1, catalase, and PRDX3 influenced HIF1α stability either via indirect but distinct effects on oxygen consumption, or alternatively via differential but direct effects on proteins that influence HIF1α regulation.

HIF1α stability under hypoxia is not regulated by reactive lipid species (RLS)

Recent studies have highlighted the potential role that RLS could play in regulating HIF transcription rather than HIF1α stability. Accordingly, we forced expression of GPX4, a selenoprotein with known ability to neutralize reactive lipid species. Despite being active in combating RLS mediated ferroptotic death in transformed cells (Figure 6H), GPX4 had no effect on HIF1α stability in hypoxia (Figures 6C and 6D) or HIF-dependent transcription (Figures 6E and 6F). These data suggest that while some RLS (e.g. tert-butyl hydroperoxide) are sufficient to activate HIF transcription, they are not necessary to stabilize HIF1α or drive HIF1α-dependent transcription in hypoxia.

HIF1α stability under hypoxia can be redox modulated by protein S-glutathionylation

Our results show that oxidants are not sufficient to activate HIF1α in hypoxia or normoxia. Nevertheless, we provide experimental support for a new model of how HIF1α stability is redox regulated in hypoxia. An increase in oxidized glutathione leads to increased *S*-glutathionylation of proteasomal subunits as a tuning signal to further modulate the amplitude of HIF PHD-mediated HIF1α stability in hypoxia. Accordingly, agents that inhibited glutathione reductase (BCNU), or increased the GSSG to GSH ratio (Diamide, GSSG methyl ester) increased HIF1α stability (ODD-luciferase activity) in hypoxia (Figure 7A). By contrast, agents known to alter the GSSG to GSH ratio in favor of reduced glutathione (e.g. GSH ethyl ester, NAC, or OTC), diminished HIF1α stability (ODD-luciferase activity) in hypoxia (Figure 7A). Oxidation of the cytoplasmic redox state in hypoxia is transduced into changes in HIF1α stability not via *S*-glutathionylation of a single known cysteine (520) in the HIF1α oxygen dependent domain (Figure 7H) or due to *S*-glutathionylation of known upstream regulators of HIF1α. Rather, direct *S*-glutathionylation of Rpn1 or Rpn2 proteins, members of the 19S regulatory particle of the 26S

proteasome, works in concert with hypoxia specific signals mediated via the HIF prolyl hydroxylases to enhance HIF1α stability (Figure 8H). Cell viability of hypoxic cells with a net oxidized cytosol is maintained as a result of HIF-dependent induction of the serine synthesis pathway and one carbon (folate cycle) metabolism in the mitochondria, which would maintain NADPH and reduced glutathione specifically in that organelle (55). Our results further suggest that the redox regulation of proteasomal activity in hypoxia may be quite different from that observed under conditions of oxidative stress in normoxia (56).

Our studies suggest that inhibitors of glutaredoxin or glutathione reductase, which would be expected to increase net *S*-glutathionylation of Rpn1 and Rpn2, and possibly other proteins, could be used as therapeutic agents to enhance HIF signaling in conditions where HIF PHD inhibitors have been effective including stroke, mitochondrial diseases, vascular dysfunction, and chronic anemia due to kidney failure. As important, the studies also suggest that the cellular redox state (as monitored by the net *S*-glutathionylation of Rpn1 and Rpn2) in transformed and non-transformed cells may provide critical gain modulation of HIF1α stability under conditions of hypoxia, and thus be important gatekeepers of this evolutionarily conserved adaptive response.

Methods

Cell lines and In Vitro Tissue Culture Studies

Immature primary cortical neurons were isolated from CD1 mice embryos (embryonic day 15 [E15]) as previously described (57) by following the protocol approved by IACUC at Weill Cornell Medicine. SH-SY5Y human neuroblastoma cells (purchased from ATCC) were cultured in DMEM/F-12 plus GlutaMAX medium added with 10% fetal bovine serum (Invitrogen) and 1% penicillin/streptomycin (Invitrogen). HeLa cells and Hep3B cells (purchased from ATCC) were

cultured in EMEM medium added with 10% fetal bovine serum (Invitrogen) and 1% penicillin/streptomycin (Invitrogen).

Islets were harvested from Sprague–Dawley male rats (~250g, Envigo, Huntingdon, Cambridgeshire, United Kingdom) anesthetized by an intraperitoneal injection of sodium pentobarbital (35 mg/230g rat). All procedures were approved by the University of Washington Institutional Animal Care and Use Committee. Islets were prepared and purified as previously described (58) and then cultured at 37°C in RPMI Media 1640 (Gibco, Grand Island, NY) supplemented with 10% heat-inactivated fetal bovine serum (Atlanta Biologicals, Lawrenceville, GA) for specified times with the adenovirus coding the H_2O_2-sensitive dye (HyPer).

Adenoviral transduction, hypoxia/normoxia exposure, and oxygen glucose deprivation (OGD)

Adenoviral constructs of MnSOD, catalase, GPX1 and respective GFP control were purchased from University of Iowa, Viral Vector Core Facility. Adenoviral construct of ddGPX4 (GPX4 with destabilization domain) and the respective GFP control were obtained from ViraQuest, Inc. (North liberty, IA) and adenoviral constructs of PRDX3, GRX1 and respective GFP control were obtained from Vector Biolabs. For GPX4 construct, we took leverage of a novel technique recently developed by Thomas Wandless group (59) to deliberately regulate the level of expression of a protein of interest. Adenoviral construct of ddGPX4 had an *E. coli* dihydrofolate reductase (ecDHFR) mutant (it was called as degradation domain) fused to its CMV promoter which displays Trimethoprim (TMP) dependent stability. Because of the fusion of degradation domain to the GPX4 promoter, GPX4 also displayed TMP dependent stability. Without TMP, GPX4 was rapidly degraded completely through proteasome but with increase in dose of TMP, GPX4 stability increases. Treatment of ddGPX4 expressing cells with 10µM TMP for 12h

stabilized ddGPX4 very well. SH-SY5Y cells, HeLa cells or Hep3B cells were transduced with different adenoviral constructs at 500 MOI (Multiplicity of infection) incubated for 72h and primary immature cortical neurons (PCNs) were transduced with different adenoviral constructs at 100 MOI (Multiplicity of infection) for 48h. The maximal expression of these constructs was determined by expressing adenoviral construct of GFP at 500 MOI for 72h in SH-SY5Y cells and 100 MOI for 48h in PCNs, respectively, on slides and staining them with GFP antibody (Abcam, ab6556). 10µM TMP was added to ddGPX4 expressing cells and their respective control GFP expressing cells after 60h of adenoviral incubation for 12h in order to get stabilized GPX4 expression. Parallel sets without transduction of adenoviral constructs but probed with same GFP antibody were used as respective negative controls in each in-vitro models (Figure S2). Thereafter, one set was kept in normoxia (21% oxygen) and a parallel set in hypoxia (1% oxygen) for 4h. For the study of changes in endogenous antioxidants, SH-SY5Y cells and primary cortical neurons were exposed to normoxia/hypoxia for a relatively longer time period, 8h so that we could visualize more clear difference under normoxic and hypoxic conditions.

In order to study real time changes in hydrogen peroxide in hypoxia condition, the adenovirus containing the cytosolic H_2O_2 sensor, pHyPer-cyto vector (FP942, Evrogen, Moscow, Russia) (36) was generated by Vector Biolabs (Malvern, PA) as previously described (60). The H_2O_2 sensor was transduced in intact islets during incubation in RPMI media supplemented with 10% heat-inactivated fetal bovine serum and the adenoviruses at 100 MOI for 3 days at 37°C as previously optimized(37). SH-SY5Y cells and Hep3B cells were also transduced with the H_2O_2 sensor at 100 MOI in a similar manner. Oxygen-glucose deprivation (OGD) is an in-vitro model of ischemia. In order to induce OGD, SH-SY5Y cells were kept in the medium without glucose and then exposed to 1% oxygen for 2 hours.

Real-time epifluorescent imaging of intracellular H_2O_2

Real-time imaging experiments were carried out while islets were perifused using a commercially available temperature-controlled Bioptechs FCS2, a closed system, parallel plate flow chamber (Butler, PA) as previously described (37). After the islets were loaded into the perifusion chambers, the chamber was sealed and mounted onto the stage of a Nikon Eclipse TE-200 inverted microscope. KRB was pumped through the perifusion chamber at flow rates of 120µl/min using a Masterflex L/S peristaltic pump (Cole-Parmer, Vernon Hills, IL). Use of an artificial gas exchanger positioned on the inflow side of the perifusion chamber enabled rapid changes in the concentrations of dissolved oxygen by switching the source tank of gas between tanks containing 21% and 1% oxygen (balance 5% carbon dioxide and nitrogen)(61, 62). The HyPer signal was generated by dual fluorescence excitation via a xenon arc lamp (Lambda LS-1620, Sutter Instrument Company, Novato, CA) through either a 405/30nm or a 480/40nm bandpass filter and detected at 510nm through a longpass dichroic mirror with a cutoff below 500nm. The images were taken using a digital camera (Photometrics Cool Snap HQ2 CCD camera, Tucson, AZ) through a 40X Super Fluor Nikon objective (DIC H/N2). Data were expressed ratiometrically, where the excitation intensities at 480nm were divided by those obtained during excitation at 405nm. Similar procedure was used for real time monitoring of H_2O_2 in SH-SY5Y cells and Hep3B cells. In order to further confirm the specificity of HyPer signals, we treated Hep3B cells with the bacterial Streptolysin-O (which creates pores in the cell membranes) to selectively permeabilize the plasma membrane followed by their exposure to increasing concentrations of exogenous H_2O_2. Real time measurement of changes in the HyPer signals in response to exogenous addition of H_2O_2 confirmed the specificity of HyPer signal with regard to H_2O_2.

Real-time epifluorescent imaging of intracellular NAD(P)H

NAD(P)H autofluorescence was measured similarly to H_2O_2, except there was no need for loading with dye, and the excitation and emission wavelengths were 360 and 460nm, respectively [as previously described (63)]. To calibrate the relative fluorescence units (RFU), at the end of experiments, the steady state RFU in the presence of potassium cyanide (KCN) and, subsequently, FCCP was measured. The normalized fluorescence of NAD(P)H was then calculated as follows,

$$\% \text{ Reduced NAD(P)H} = 100 * (RFU_{test} - RFU_{FCCP})/(RFU_{KCN} - RFU_{FCCP}) \quad \text{(Eq. 1)}$$

where RFU_{FCCP} and RFU_{KCN} equals the average of the final 10 time points during which each agent was present.

Real-time measurement of insulin secretion rate

Outflow fractions from the flow system containing islets were collected in a fraction collection for subsequent measurement of insulin [described previously (58, 61, 62). Insulin secretion rate was calculated as the flow rate (80ul/min) times the insulin concentration in the outflow Fractions, over the number of islets in the chamber [typically 50 (64)]. Insulin was measured by radioimmunoassay (RI-13K, EMD Millipore, Darmstadt, Germany) as per the manufacturer instructions.

ODD-luciferase activity assay

The ODD-luciferase construct with pcDNA3.1 plasmid vector was constructed as previously described (65). The proline p402 and p564 present within the oxygen degradation domain (ODD) of HIF1α, when hydroxylated by HIF-PHDs, allow its binding to the VHL protein that target it for proteasomal degradation. In this way, the stabilization of ODD can be used as a marker of HIF1α stability (39, 65). Because of the luciferase tagged with ODD, the increase in ODD stability leads

to a proportional increase in the luciferase activity and this provides a very good way of measuring the HIF1α stability in a quantitative manner with a wide dynamic range. To this end, we used SH-SY5Y cells stably expressing ODD-luciferase. These cells were made by co-transfecting ODD-luciferase plasmid along with a puromycin resistance plasmid in SH-SY5Y cells and stably transfected cells were positively selected in presence of 4µg/ml of puromycin. Luciferase activity was measured by luciferase assay kit (promega) using an LMaxII™ microplate luminometer (molecular Devices). ODD-luciferase activity was normalized to the protein content of each well measured by Bio-Rad DC™ protein assay kit.

Gene expression study

Total RNA was prepared from SH-SY5Y cells using the Nucleospin RNA kit (MACHEREY-NAGEL) and following their protocol. Real time PCRs were performed as a duplex reaction using FAM labeled *Enolase2* (Human - Hs00157360_m1), *Bnip3* (Human - Hs00969291_m1), and *Hif1α* (Human - Hs00153153_m1) gene expression assays (Thermo Fisher Scientific) and VIC labeled *human β actin* endogenous control probe (Human - 4326315E) or *RNA28S5* (Human - Hs03654441_s1) (Thermo Fisher Scientific) so that amplified mRNA can be normalized to *β actin* or *RNA28S5*. These experiments were performed using a 7500 Rea-time PCR system (Applied Biosystems) using standard PCR protocol and amplification conditions.

In order to measure gene expression in pancreatic islets exposed to normoxia or hypoxia, islets were first placed in incubators containing either 21% or 1% oxygen for 2h. At the end of this time, islets were lysed and total RNA was purified using RNeasy Mini Kit (Qiagen, Hilden Germany). *Bnip3*, *Kdm6b* and *rat Actin B* mRNA were measured by quantitative PCR using FAM labeled *Bnip3* (Rat - Rn00821446_g1), *Kdm6b* (Rat - Rn01471506_m1) gene expression assays and VIC labeled *rat β actin* endogenous control probe (Rat - 4352340E), all purchased from

Thermo Fisher Scientific. These experiments were performed on Mx3005P® Multiplex QPCR System (Stratagene, La Jolla, CA) with samples loaded in triplicate using ~ 100ng of total RNA.

Enzyme activity assay

For GPX1, catalase, and MnSOD activity assay, cells in each sample expressing respective adenoviral constructs were collected, lysed and used for respective enzyme activity assay following the protocols of GPX1, catalase, and SOD assay kit from Biovision. Total protein was measured using the Bio-Rad DC protein assay kit. The enzyme activity was normalized to the protein concentration for each sample.

Cell viability assay

In order to test the functional activity of GPX4, immature primary cortical neurons (E15) were isolated from mice embryos and plated at 10^6 cells/ml in 96 well plate. The next day, cells were transduced with GPX4 adenoviral constructs at 100 MOI. After 24h incubation, cells were treated with glutamate analog, homocysteic acid (HCA) (5mM) which inhibits Xc^- transporter, thereby inhibiting cysteine uptake which leads to glutathione depletion and increase in intracellular oxidative stress. Cells were also treated with 10µM TMP at the same time to stabilize GPX4 protein. The next day, cell viability was assessed by the MTT assay (Promega) to understand whether ddGPX4 is functionally active to show its protective effect by decreasing oxidants under oxidative stress.

ROS measurement through DCF flow cytometry

To measure changes in ROS levels, molecular probe DCFDA (2', 7' – dichlorofluorescin diacetate) was used. SH-SY5Y cells in normoxia as well as hypoxia were loaded with 20µM DCFDA for 30min. DCFDA diffuses through the cell membrane and is deacetylated by intracellular esterases to a non-fluorescent form which is later oxidized by ROS into 2', 7' –

dichlorofluorescein (DCF) which is a highly fluorescent compound. Thereafter, parallel sets of cells in normoxia as well as hypoxia were treated with 5mM H_2O_2 for 30min and were considered as positive controls. After incubation, fluorescence was measured through flow cytometry at the wavelength of excitation, 485nm and emission, 535nm, respectively. Production of ROS was measured as mean fluorescence index multiplied by respective cell counts and was expressed as fold change with respect to control.

Immunoblotting and Immunoprecipitation

Protein extracts were prepared using 1% triton buffer containing protease inhibitor, separated by SDS-PAGE, transferred onto nitrocellulose membrane and probed with antibodies against GFP (Cell Signaling Technology; 2555), MnSOD (Sigma-Aldrich; HPA001814), catalase (Sigma-Aldrich; C0979), GPX1 (Cell Signaling Technology; 3286S and Novus Biologicals; NBP1-33620), GPX4 (LSBio; LS B1596), PRDX3 (Novus Biologicals; NBP2-19777), Luciferase (Santa Cruz Biotechnology; sc-74548), HIF1α (Novus Biologicals; NB100-479), Citrate synthase (Cell Signaling Technology; 14309S), Glutathione (Abcam; ab19534), GRX1 (Abcam; ab45953) and β-actin (Sigma-Aldrich; A2066 and A5316). Rpn10 (Cell Signaling Technology; 12441S) and Rpn13 (Abcam; ab157185) antibodies were used for Immunoprecipitation and Rpn1 (Santa Cruz Biotechnology; sc-271584), Rpn2 (Enzo Life Sciences; BML-PW9270-0100), and ubiquitin (Santa Cruz Biotechnology; sc-8017) antibodies were used for immunoblotting.

Proteasome activity Assay

The proteasome activity was measured by using a 26S proteasome activity kit (Millipore; APT 280), as described by the manufacturer's instructions. SH-SY5Y cells or primary cortical neurons were incubated either in normoxia or hypoxia in parallel sets for 4h and then media was taken out and cells were washed with 1X PBS twice. Thereafter, cell pellets were collected by

centrifugation at 1500 rcf for 5min at 4°C. Then, cell pellets were lysed with the lysis buffer containing 50mM HEPES (pH 7.5), 5mM EDTA, 150mM NaCl and 1% Triton X-100. 2mM ATP (Catalog Number: BML-EW9805-0125) was also added to the lysis buffer to improve the recovery of 26S proteasome. Cells were lysed by incubating the lysate for 30 min on ice with vortexing at 10min intervals. Thereafter, lysates were centrifuged at 15,000 rpm for 15 min at 4°C. The clear supernatants were collected in clean microcentrifuge tubes and were used for the proteasome activity assay. Then, 100 µL of reaction mixture containing 10 µL of 10X assay buffer and 10 µL of 500 µM proteasome substrate provided with the kit, 10 µL of respective lysate and remaining water was prepared for each sample (prepared in triplicate for each sample) and was incubated for 1 h at 37 °C. Fluorogenic peptide used as substrate was Leu-Leu-Val-Tyr-7-amino-4-methylcoumarin (LLVY-AMC at 500 µM). 10 µL of positive control provided with the kit was also incubated with the reaction mixture containing 10 µL of 10X buffer and 10 µL of 500 µM proteasome substrate for 1 h at 37 °C. The reaction mixture without cell lysate was used as blank, and proteasome activities were measured by quantification of relative fluorescent units from the release of the fluorescent-cleaved products aminomethylcoumarin (AMC) (at 380/460 nm) using a microplate reader (SpectraMax Plus 384, Molecular Devices).

Identification and Label-free quantitation (LFQ) of protein *S*-glutathionylation by Orbitrap Fusion under FT-Q-IT mode

Sample preparation

The sample preparations for protein *S*-glutathionylation identification were conducted as described previously (66) with slight modifications. Specifically, equal amount of protein (300µg) from each sample were suspended and denatured at 1.0µg/µl in alkylation buffer consisting of 250mM HEPES (pH7.4), 20mM NEM, 2% SDS, 1mM sodium ascorbate and 1mM CuCl. The

alkylation reaction was carried out in 0.5ml Amicon Ultra 10K molecular weight cut off (MWCO) filter units (EMD Millipore) in the dark, at 55°C for 30 min. Proteins were diluted to ~1.0 µg/µl in 25mM HEPES (pH7.7), followed by the addition of 2.5µg/ml GRX1 (*E. coli* glutaredoxin from Sigma), 0.5mM GSH (from Sigma), 1mM beta-NADPH.4Na (from Thermo Fisher), and 4U/ml of GR (Glutathione reductase from Roche Diagnostics Corporation). Samples were incubated at 37°C for 10 min.

Enrichment by Sepharose 6B resin and on-resin tryptic digestion, and peptide elution

Deglutathionylated proteins were diluted to ~ 120µl with 25mM HEPES (pH 7.7) buffer with 0.2% SDS and loaded to Handee Mini-Spin columns (from Pierce) containing with 35mg of prewashed thiopropyl Sepharose 6B resin (from GE Healthcare). Enrichment was carried out in a mixer at room temperature with shaking at 500 rpm for 2 h. On-resin protein digestion was carried out at 37°C overnight in ~120µl of digestion buffer containing 25mM HEPES (pH7.7) with added 12µg trypsin (Promega, Madison, WI) at ~1:25 w/w. Cysteine containing peptides (Cys-peptides) were eluted by incubation with 20mM dithiothreitol (DTT) in 100µl of 25mM ammonium bicarbonate pH 8.0 twice at room temperature for 30 and 10min, respectively. All eluted Cys-peptide samples were combined, dried down and reconstituted with alkylation buffer: 50mM TEAB, pH 8.5, 60 mM iodoacetamide for 30min in the dark at room temperature, then quenched with a final concentration of 43mM DTT. The samples were evaporated to dryness by a Speedvac SC110 (Thermo Savant, Milford, MA) and suspended in 0.5% formic acid for subsequent nanoLC-MS/MS analysis.

Identification and LFQ of S-glutathionylated peptides by nano LC/MS/MS Analysis

The nano LC-ESI-MS/MS analysis was carried out using an Orbitrap Fusion™ Tribrid™ (Thermo-Fisher Scientific, San Jose, CA) mass spectrometer equipped with a nanospray Flex

Ion Source, and coupled with a Dionex UltiMate3000RSLCnano system (Thermo, Sunnyvale, CA) as reported previously(67). The peptide samples (5µl) were injected onto a PepMap C18 trap column-nano Viper (5µm, 100µm x 2cm, Thermo) at 20µl/min flow rate for on-line desalting and then separated on a PepMap C-18 RP nano column (3µm, 75µm x 25cm) at 35°C, and eluted in a 90min gradient of 5% to 38% acetonitrile (ACN) in 0.1% formic acid at 300nl/min., followed by a 7min ramping to 90% ACN-0.1% FA and an 8min hold at 90% ACN-0.1% FA. The column was re-equilibrated with 0.1% FA for 25min prior to the next run. The Orbitrap Fusion is operated in positive ion mode with spray voltage set at 1.6 kV and source temperature at 275°C. External calibration for FT, IT and quadrupole mass analyzers was performed. In data-dependent acquisition (DDA) analysis, the instrument was operated using FT mass analyzer in MS scan to select precursor ions followed by 3 second "Top Speed" data-dependent CID ion trap MS/MS scans at 1.6 m/z quadrupole isolation for precursor peptides with multiple charged ions above a threshold ion count of 10,000 and normalized collision energy of 30%. All data were acquired under Xcalibur 3.0 operation software (Thermo-Fisher Scientific).

Data analysis

The DDA files for MS and MS/MS raw spectra were subjected to database searches using Proteome Discoverer (PD) 2.2 software (Thermo Fisher Scientific, Bremen, Germany) with the Sequest HT algorithm for both identification and LFQ. The database search was conducted against Human UnitProt database that contained 20,153 entries with two-missed trypsin cleavage sites allowed. The peptide precursor tolerance was set to 10 ppm and fragment ion tolerance was set to 0.6 Da. Oxidation of M, deamidation of N and Q, and acetylation of protein N-terminus were specified as dynamic modifications of amino acid residues. Carbamidomethyl Cys and NEM Cys were also specified as a variable modification. Only high confidence peptides

defined by Sequest HT with a 1% FDR by Percolator were considered for the peptide identification.

In our strategy for indirect identification of *S*-glutathionylation, these peptides with Cys residues being carbamidomethylated should be the *S*-glutathionylated peptides/residues. For relative quantitation analysis of S-glutathionylated peptides in four different groups, 6 raw files from two groups (Samples between 3 triplicate controls in normoxia and the 3 triplicate test samples in hypoxia) were searched together with setting ratio of test/control for each LFQ comparison based on the MS1 intensity of *S*-glutathionylated peptides in each sample without normalization.

Quantification and Statistical Analysis

All experiments were performed as at least three independent sets and data were displayed as means ± standard deviation (SD). Statistical significance were assessed in GraphPad Prism using either Student's t tests to compare values between two specific groups or one-way ANOVA followed by Dunnett's post-hoc test/Tukey's Post-hoc test to compare the values of more than two groups or two-way ANOVA followed by Bonferroni's post-hoc test to compare the values of two groups under two different conditions at a given time. Statistical details for each figures can be found in their respective figure legends. The p value of 0.05 or less was considered statistically significant in all of statistical analyses.

Acknowledgements

This work was supported by the National Institute of Health (Grant P01 AG14930-15A1, Project 1 to RRR), by Dr. Miriam and Sheldon G. Adelson Medical Research Foundation grant to RRR, by a Goldsmith Fellowship to Amit Kumar for transition to independence, by Diabetes Research Center Cell Function Analysis Core (P30 DK17047; University of Washington) to Ian Sweet and

by NIH SIG grant 1S10 OD017992-01 grant support to Sheng Zhang for the Orbitrap Fusion mass spectrometer. We thank the Proteomic and MS Facility of Cornell University for providing the mass spectrometry data. We also want to thank Sunghee Cho and Jiwon Yang for their help in data acquisition through flow cytometry. We would like to acknowledge critical comments and suggestions from Drs. Ratcliffe, Schofield, Semenza, Silva and Ciechanover. The authors declare no competing financial interests.

Author Contributions

AK and RRR conceived and designed the research and AK performed most of the experiments. MV performed some initial experiments and SSK helped in optimizing HIF1α blot. IG helped with enzyme activity assay, AAS helped with ROS measurement and JTP helped with glutathione redox measurement. AR, WW and IRS performed experiments in islets and helped with writing the same part in the manuscript. ETA and SZ helped with mass-spectrometry studies. AK analyzed, compiled the data and prepared figures. JWC helped with the preparation of figures. AK and RRR wrote the manuscript. All co-authors discussed the results and contributed in the final editing of the manuscript.

Declaration of Interests

The authors declare no competing financial interests.

References

1. Jain M, Rivera S, Monclus EA, Synenki L, Zirk A, Eisenbart J, et al. Mitochondrial reactive oxygen species regulate transforming growth factor-beta signaling. The Journal of biological chemistry. 2013 Jan 11;288(2):770-7. PubMed PMID: 23204521. Pubmed Central PMCID: 3543026.
2. Lei H, Kazlauskas A. A reactive oxygen species-mediated, self-perpetuating loop persistently activates platelet-derived growth factor receptor alpha. Molecular and cellular biology. 2014 Jan;34(1):110-22. PubMed PMID: 24190966. Pubmed Central PMCID: 3911282.
3. Hameed LS, Berg DA, Belnoue L, Jensen LD, Cao Y, Simon A. Environmental changes in oxygen tension reveal ROS-dependent neurogenesis and regeneration in the adult newt brain. eLife. 2015 Oct 20;4. PubMed PMID: 26485032. Pubmed Central PMCID: 4635398.
4. Bae YS, Kang SW, Seo MS, Baines IC, Tekle E, Chock PB, et al. Epidermal growth factor (EGF)-induced generation of hydrogen peroxide. Role in EGF receptor-mediated tyrosine phosphorylation. The Journal of biological chemistry. 1997 Jan 03;272(1):217-21. PubMed PMID: 8995250.
5. Lee SR, Kwon KS, Kim SR, Rhee SG. Reversible inactivation of protein-tyrosine phosphatase 1B in A431 cells stimulated with epidermal growth factor. The Journal of biological chemistry. 1998 Jun 19;273(25):15366-72. PubMed PMID: 9624118.
6. Salmeen A, Andersen JN, Myers MP, Meng TC, Hinks JA, Tonks NK, et al. Redox regulation of protein tyrosine phosphatase 1B involves a sulphenyl-amide intermediate. Nature. 2003 Jun 12;423(6941):769-73. PubMed PMID: 12802338.
7. Semenza GL, Wang GL. A nuclear factor induced by hypoxia via de novo protein synthesis binds to the human erythropoietin gene enhancer at a site required for transcriptional

activation. Molecular and cellular biology. 1992 Dec;12(12):5447-54. PubMed PMID: 1448077. Pubmed Central PMCID: 360482.

8. Wang GL, Semenza GL. General involvement of hypoxia-inducible factor 1 in transcriptional response to hypoxia. Proceedings of the National Academy of Sciences of the United States of America. 1993 May 01;90(9):4304-8. PubMed PMID: 8387214. Pubmed Central PMCID: 46495.
9. Wang GL, Jiang BH, Rue EA, Semenza GL. Hypoxia-inducible factor 1 is a basic-helix-loop-helix-PAS heterodimer regulated by cellular O2 tension. Proceedings of the National Academy of Sciences of the United States of America. 1995 Jun 06;92(12):5510-4. PubMed PMID: 7539918. Pubmed Central PMCID: 41725.
10. Maxwell PH, Wiesener MS, Chang GW, Clifford SC, Vaux EC, Cockman ME, et al. The tumour suppressor protein VHL targets hypoxia-inducible factors for oxygen-dependent proteolysis. Nature. 1999 May 20;399(6733):271-5. PubMed PMID: 10353251.
11. Jaakkola P, Mole DR, Tian YM, Wilson MI, Gielbert J, Gaskell SJ, et al. Targeting of HIF-alpha to the von Hippel-Lindau ubiquitylation complex by O2-regulated prolyl hydroxylation. Science. 2001 Apr 20;292(5516):468-72. PubMed PMID: 11292861.
12. Ivan M, Kondo K, Yang H, Kim W, Valiando J, Ohh M, et al. HIFalpha targeted for VHL-mediated destruction by proline hydroxylation: implications for O2 sensing. Science. 2001 Apr 20;292(5516):464-8. PubMed PMID: 11292862.
13. Epstein AC, Gleadle JM, McNeill LA, Hewitson KS, O'Rourke J, Mole DR, et al. C. elegans EGL-9 and mammalian homologs define a family of dioxygenases that regulate HIF by prolyl hydroxylation. Cell. 2001 Oct 05;107(1):43-54. PubMed PMID: 11595184.

14. Ivan M, Haberberger T, Gervasi DC, Michelson KS, Gunzler V, Kondo K, et al. Biochemical purification and pharmacological inhibition of a mammalian prolyl hydroxylase acting on hypoxia-inducible factor. Proceedings of the National Academy of Sciences of the United States of America. 2002 Oct 15;99(21):13459-64. PubMed PMID: 12351678. Pubmed Central PMCID: 129695.
15. Wood SM, Gleadle JM, Pugh CW, Hankinson O, Ratcliffe PJ. The role of the aryl hydrocarbon receptor nuclear translocator (ARNT) in hypoxic induction of gene expression. Studies in ARNT-deficient cells. The Journal of biological chemistry. 1996 Jun 21;271(25):15117-23. PubMed PMID: 8662957.
16. Jiang BH, Rue E, Wang GL, Roe R, Semenza GL. Dimerization, DNA binding, and transactivation properties of hypoxia-inducible factor 1. The Journal of biological chemistry. 1996 Jul 26;271(30):17771-8. PubMed PMID: 8663540.
17. Weidemann A, Bernhardt WM, Klanke B, Daniel C, Buchholz B, Campean V, et al. HIF activation protects from acute kidney injury. J Am Soc Nephrol. 2008 Mar;19(3):486-94. PubMed PMID: 18256363. Pubmed Central PMCID: 2391048.
18. Conde E, Alegre L, Blanco-Sanchez I, Saenz-Morales D, Aguado-Fraile E, Ponte B, et al. Hypoxia inducible factor 1-alpha (HIF-1 alpha) is induced during reperfusion after renal ischemia and is critical for proximal tubule cell survival. PloS one. 2012;7(3):e33258. PubMed PMID: 22432008. Pubmed Central PMCID: 3303832.
19. Semenza GL. Hypoxia-inducible factor 1 and cardiovascular disease. Annu Rev Physiol. 2014;76:39-56. PubMed PMID: 23988176. Pubmed Central PMCID: 4696033.
20. Sheldon RA, Lee CL, Jiang X, Knox RN, Ferriero DM. Hypoxic preconditioning protection is eliminated in HIF-1alpha knockout mice subjected to neonatal hypoxia-ischemia. Pediatric

research. 2014 Jul;76(1):46-53. PubMed PMID: 24713818. Pubmed Central PMCID: 4167022.

21. Semenza GL. Hypoxia-inducible factors: mediators of cancer progression and targets for cancer therapy. Trends Pharmacol Sci. 2012 Apr;33(4):207-14. PubMed PMID: 22398146. Pubmed Central PMCID: 3437546.
22. Bryant AJ, Carrick RP, McConaha ME, Jones BR, Shay SD, Moore CS, et al. Endothelial HIF signaling regulates pulmonary fibrosis-associated pulmonary hypertension. Am J Physiol Lung Cell Mol Physiol. 2016 Feb 1;310(3):L249-62. PubMed PMID: 26637636. Pubmed Central PMCID: 4838140.
23. Chandel NS, McClintock DS, Feliciano CE, Wood TM, Melendez JA, Rodriguez AM, et al. Reactive oxygen species generated at mitochondrial complex III stabilize hypoxia-inducible factor-1alpha during hypoxia: a mechanism of O2 sensing. The Journal of biological chemistry. 2000 Aug 18;275(33):25130-8. PubMed PMID: 10833514.
24. Brunelle JK, Bell EL, Quesada NM, Vercauteren K, Tiranti V, Zeviani M, et al. Oxygen sensing requires mitochondrial ROS but not oxidative phosphorylation. Cell metabolism. 2005 Jun;1(6):409-14. PubMed PMID: 16054090.
25. Mansfield KD, Guzy RD, Pan Y, Young RM, Cash TP, Schumacker PT, et al. Mitochondrial dysfunction resulting from loss of cytochrome c impairs cellular oxygen sensing and hypoxic HIF-alpha activation. Cell metabolism. 2005 Jun;1(6):393-9. PubMed PMID: 16054088. Pubmed Central PMCID: 3141219.
26. Bell EL, Klimova TA, Eisenbart J, Moraes CT, Murphy MP, Budinger GR, et al. The Qo site of the mitochondrial complex III is required for the transduction of hypoxic signaling via reactive

oxygen species production. The Journal of cell biology. 2007 Jun 18;177(6):1029-36. PubMed PMID: 17562787. Pubmed Central PMCID: 2064363.

27. Emerling BM, Platanias LC, Black E, Nebreda AR, Davis RJ, Chandel NS. Mitochondrial reactive oxygen species activation of p38 mitogen-activated protein kinase is required for hypoxia signaling. Molecular and cellular biology. 2005 Jun;25(12):4853-62. PubMed PMID: 15923604. Pubmed Central PMCID: 1140591.
28. Agani FH, Pichiule P, Chavez JC, LaManna JC. The role of mitochondria in the regulation of hypoxia-inducible factor 1 expression during hypoxia. The Journal of biological chemistry. 2000 Nov 17;275(46):35863-7. PubMed PMID: 10961998.
29. Taylor CT. Mitochondria and cellular oxygen sensing in the HIF pathway. The Biochemical journal. 2008 Jan 1;409(1):19-26. PubMed PMID: 18062771.
30. Doege K, Heine S, Jensen I, Jelkmann W, Metzen E. Inhibition of mitochondrial respiration elevates oxygen concentration but leaves regulation of hypoxia-inducible factor (HIF) intact. Blood. 2005 Oct 01;106(7):2311-7. PubMed PMID: 15947089.
31. Hagen T, Taylor CT, Lam F, Moncada S. Redistribution of intracellular oxygen in hypoxia by nitric oxide: effect on HIF1alpha. Science. 2003 Dec 12;302(5652):1975-8. PubMed PMID: 14671307.
32. Chua YL, Dufour E, Dassa EP, Rustin P, Jacobs HT, Taylor CT, et al. Stabilization of hypoxia-inducible factor-1alpha protein in hypoxia occurs independently of mitochondrial reactive oxygen species production. The Journal of biological chemistry. 2010 Oct 08;285(41):31277-84. PubMed PMID: 20675386. Pubmed Central PMCID: 2951202.
33. Christman MF, Storz G, Ames BN. OxyR, a positive regulator of hydrogen peroxide-inducible genes in Escherichia coli and Salmonella typhimurium, is homologous to a family of bacterial

regulatory proteins. Proceedings of the National Academy of Sciences of the United States of America. 1989 May;86(10):3484-8. PubMed PMID: 2471187. Pubmed Central PMCID: 287162.

34. Aminova LR, Siddiq A, Ratan RR. Antioxidants, HIF prolyl hydroxylase inhibitors or short interfering RNAs to BNIP3 or PUMA, can prevent prodeath effects of the transcriptional activator, HIF-1alpha, in a mouse hippocampal neuronal line. Antioxidants & redox signaling. 2008 Dec;10(12):1989-98. PubMed PMID: 18774900. Pubmed Central PMCID: 2612757.
35. Zhang H, Bosch-Marce M, Shimoda LA, Tan YS, Baek JH, Wesley JB, et al. Mitochondrial autophagy is an HIF-1-dependent adaptive metabolic response to hypoxia. The Journal of biological chemistry. 2008 Apr 18;283(16):10892-903. PubMed PMID: 18281291. Pubmed Central PMCID: 2447655.
36. Belousov VV, Fradkov AF, Lukyanov KA, Staroverov DB, Shakhbazov KS, Terskikh AV, et al. Genetically encoded fluorescent indicator for intracellular hydrogen peroxide. Nature methods. 2006 Apr;3(4):281-6. PubMed PMID: 16554833.
37. Neal A, Rountree A, Kernan K, Van Yserloo B, Zhang H, Reed BJ, et al. Real-time imaging of intracellular hydrogen peroxide in pancreatic islets. The Biochemical journal. 2016 Dec 01;473(23):4443-56. PubMed PMID: 27729543.
38. Choudhry H, Harris AL. Advances in Hypoxia-Inducible Factor Biology. Cell metabolism. 2018 Feb 6;27(2):281-98. PubMed PMID: 29129785.
39. Smirnova NA, Rakhman I, Moroz N, Basso M, Payappilly J, Kazakov S, et al. Utilization of an in vivo reporter for high throughput identification of branched small molecule regulators of hypoxic adaptation. Chem Biol. 2010 Apr 23;17(4):380-91. PubMed PMID: 20416509. Pubmed Central PMCID: PMC4327942. Epub 2010/04/27.

40. Karuppagounder SS, Basso M, Sleiman SF, Ma TC, Speer RE, Smirnova NA, et al. In vitro ischemia suppresses hypoxic induction of hypoxia-inducible factor-1alpha by inhibition of synthesis and not enhanced degradation. Journal of neuroscience research. 2013 Aug;91(8):1066-75. PubMed PMID: 23456821. Pubmed Central PMCID: 4321689.
41. Ema M, Hirota K, Mimura J, Abe H, Yodoi J, Sogawa K, et al. Molecular mechanisms of transcription activation by HLF and HIF1alpha in response to hypoxia: their stabilization and redox signal-induced interaction with CBP/p300. The EMBO journal. 1999 Apr 1;18(7):1905-14. PubMed PMID: 10202154. Pubmed Central PMCID: 1171276.
42. Lando D, Peet DJ, Gorman JJ, Whelan DA, Whitelaw ML, Bruick RK. FIH-1 is an asparaginyl hydroxylase enzyme that regulates the transcriptional activity of hypoxia-inducible factor. Genes & development. 2002 Jun 15;16(12):1466-71. PubMed PMID: 12080085. Pubmed Central PMCID: 186346.
43. Sang N, Fang J, Srinivas V, Leshchinsky I, Caro J. Carboxyl-terminal transactivation activity of hypoxia-inducible factor 1 alpha is governed by a von Hippel-Lindau protein-independent, hydroxylation-regulated association with p300/CBP. Molecular and cellular biology. 2002 May;22(9):2984-92. PubMed PMID: 11940656. Pubmed Central PMCID: 133771.
44. Aminova LR, Chavez JC, Lee J, Ryu H, Kung A, Lamanna JC, et al. Prosurvival and prodeath effects of hypoxia-inducible factor-1alpha stabilization in a murine hippocampal cell line. The Journal of biological chemistry. 2005 Feb 04;280(5):3996-4003. PubMed PMID: 15557337.
45. Poitz DM, Augstein A, Hesse K, Christoph M, Ibrahim K, Braun-Dullaeus RC, et al. Regulation of the HIF-system in human macrophages--differential regulation of HIF-alpha subunits under sustained hypoxia. Mol Immunol. 2014 Feb;57(2):226-35. PubMed PMID: 24176785.

46. Masson N, Singleton RS, Sekirnik R, Trudgian DC, Ambrose LJ, Miranda MX, et al. The FIH hydroxylase is a cellular peroxide sensor that modulates HIF transcriptional activity. EMBO reports. 2012 Mar 01;13(3):251-7. PubMed PMID: 22310300. Pubmed Central PMCID: 3323130.
47. Tan S, Wood M, Maher P. Oxidative stress induces a form of programmed cell death with characteristics of both apoptosis and necrosis in neuronal cells. Journal of neurochemistry. 1998 Jul;71(1):95-105. PubMed PMID: 9648855.
48. Jeon D, Park HJ, Kim HS. Protein S-glutathionylation induced by hypoxia increases hypoxia-inducible factor-1alpha in human colon cancer cells. Biochemical and biophysical research communications. 2018 Jan 1;495(1):212-6. PubMed PMID: 29113799.
49. Mieyal JJ, Chock PB. Posttranslational modification of cysteine in redox signaling and oxidative stress: Focus on s-glutathionylation. Antioxidants & redox signaling. 2012 Mar 15;16(6):471-5. PubMed PMID: 22136616. Pubmed Central PMCID: 3270050.
50. Tajima M, Kurashima Y, Sugiyama K, Ogura T, Sakagami H. The redox state of glutathione regulates the hypoxic induction of HIF-1. Eur J Pharmacol. 2009 Mar 15;606(1-3):45-9. PubMed PMID: 19374849.
51. Watanabe Y, Murdoch CE, Sano S, Ido Y, Bachschmid MM, Cohen RA, et al. Glutathione adducts induced by ischemia and deletion of glutaredoxin-1 stabilize HIF-1alpha and improve limb revascularization. Proceedings of the National Academy of Sciences of the United States of America. 2016 May 24;113(21):6011-6. PubMed PMID: 27162359. Pubmed Central PMCID: 4889374.

52. Zmijewski JW, Banerjee S, Abraham E. S-glutathionylation of the Rpn2 regulatory subunit inhibits 26 S proteasomal function. The Journal of biological chemistry. 2009 Aug 14;284(33):22213-21. PubMed PMID: 19549781. Pubmed Central PMCID: 2755946.
53. Chandel NS, Maltepe E, Goldwasser E, Mathieu CE, Simon MC, Schumacker PT. Mitochondrial reactive oxygen species trigger hypoxia-induced transcription. Proceedings of the National Academy of Sciences of the United States of America. 1998 Sep 29;95(20):11715-20. PubMed PMID: 9751731. Pubmed Central PMCID: 21706.
54. Naranjo-Suarez S, Carlson BA, Tsuji PA, Yoo MH, Gladyshev VN, Hatfield DL. HIF-independent regulation of thioredoxin reductase 1 contributes to the high levels of reactive oxygen species induced by hypoxia. PloS one. 2012;7(2):e30470. PubMed PMID: 22348009. Pubmed Central PMCID: 3278416.
55. Samanta D, Park Y, Andrabi SA, Shelton LM, Gilkes DM, Semenza GL. PHGDH Expression Is Required for Mitochondrial Redox Homeostasis, Breast Cancer Stem Cell Maintenance, and Lung Metastasis. Cancer research. 2016 Aug 1;76(15):4430-42. PubMed PMID: 27280394.
56. Demasi M, Netto LE, Silva GM, Hand A, de Oliveira CL, Bicev RN, et al. Redox regulation of the proteasome via S-glutathionylation. Redox biology. 2013 Dec 14;2:44-51. PubMed PMID: 24396728. Pubmed Central PMCID: 3881202.
57. Ratan RR, Murphy TH, Baraban JM. Oxidative stress induces apoptosis in embryonic cortical neurons. Journal of neurochemistry. 1994 Jan;62(1):376-9. PubMed PMID: 7903353.
58. Sweet IR, Cook DL, DeJulio E, Wallen AR, Khalil G, Callis J, et al. Regulation of ATP/ADP in pancreatic islets. Diabetes. 2004 Feb;53(2):401-9. PubMed PMID: 14747291.

59. Iwamoto M, Bjorklund T, Lundberg C, Kirik D, Wandless TJ. A general chemical method to regulate protein stability in the mammalian central nervous system. Chemistry & biology. 2010 Sep 24;17(9):981-8. PubMed PMID: 20851347. Pubmed Central PMCID: 2943492.
60. Karamanlidis G, Lee CF, Garcia-Menendez L, Kolwicz SC, Jr., Suthammarak W, Gong G, et al. Mitochondrial complex I deficiency increases protein acetylation and accelerates heart failure. Cell metabolism. 2013 Aug 06;18(2):239-50. PubMed PMID: 23931755. Pubmed Central PMCID: 3779647.
61. Sweet IR, Cook DL, Wiseman RW, Greenbaum CJ, Lernmark A, Matsumoto S, et al. Dynamic perifusion to maintain and assess isolated pancreatic islets. Diabetes Technol Ther. 2002;4(1):67-76. PubMed PMID: 12017423.
62. Sweet IR, Khalil G, Wallen AR, Steedman M, Schenkman KA, Reems JA, et al. Continuous measurement of oxygen consumption by pancreatic islets. Diabetes Technol Ther. 2002;4(5):661-72. PubMed PMID: 12450449.
63. Gilbert M, Jung SR, Reed BJ, Sweet IR. Islet oxygen consumption and insulin secretion tightly coupled to calcium derived from L-type calcium channels but not from the endoplasmic reticulum. The Journal of biological chemistry. 2008 Sep 05;283(36):24334-42. PubMed PMID: 18593707. Pubmed Central PMCID: 2528984.
64. Sweet IR, Gilbert M. Contribution of calcium influx in mediating glucose-stimulated oxygen consumption in pancreatic islets. Diabetes. 2006 Dec;55(12):3509-19. PubMed PMID: 17130499.
65. Safran M, Kim WY, O'Connell F, Flippin L, Gunzler V, Horner JW, et al. Mouse model for noninvasive imaging of HIF prolyl hydroxylase activity: assessment of an oral agent that stimulates erythropoietin production. Proceedings of the National Academy of Sciences of the

United States of America. 2006 Jan 03;103(1):105-10. PubMed PMID: 16373502. Pubmed Central PMCID: 1324998.

66. Su D, Gaffrey MJ, Guo J, Hatchell KE, Chu RK, Clauss TR, et al. Proteomic identification and quantification of S-glutathionylation in mouse macrophages using resin-assisted enrichment and isobaric labeling. Free radical biology & medicine. 2014 Feb;67:460-70. PubMed PMID: 24333276. Pubmed Central PMCID: 3945121.

67. Thomas CJ, Cleland TP, Zhang S, Gundberg CM, Vashishth D. Identification and characterization of glycation adducts on osteocalcin. Anal Biochem. 2017 May 15;525:46-53. PubMed PMID: 28237256. Pubmed Central PMCID: 5490980.

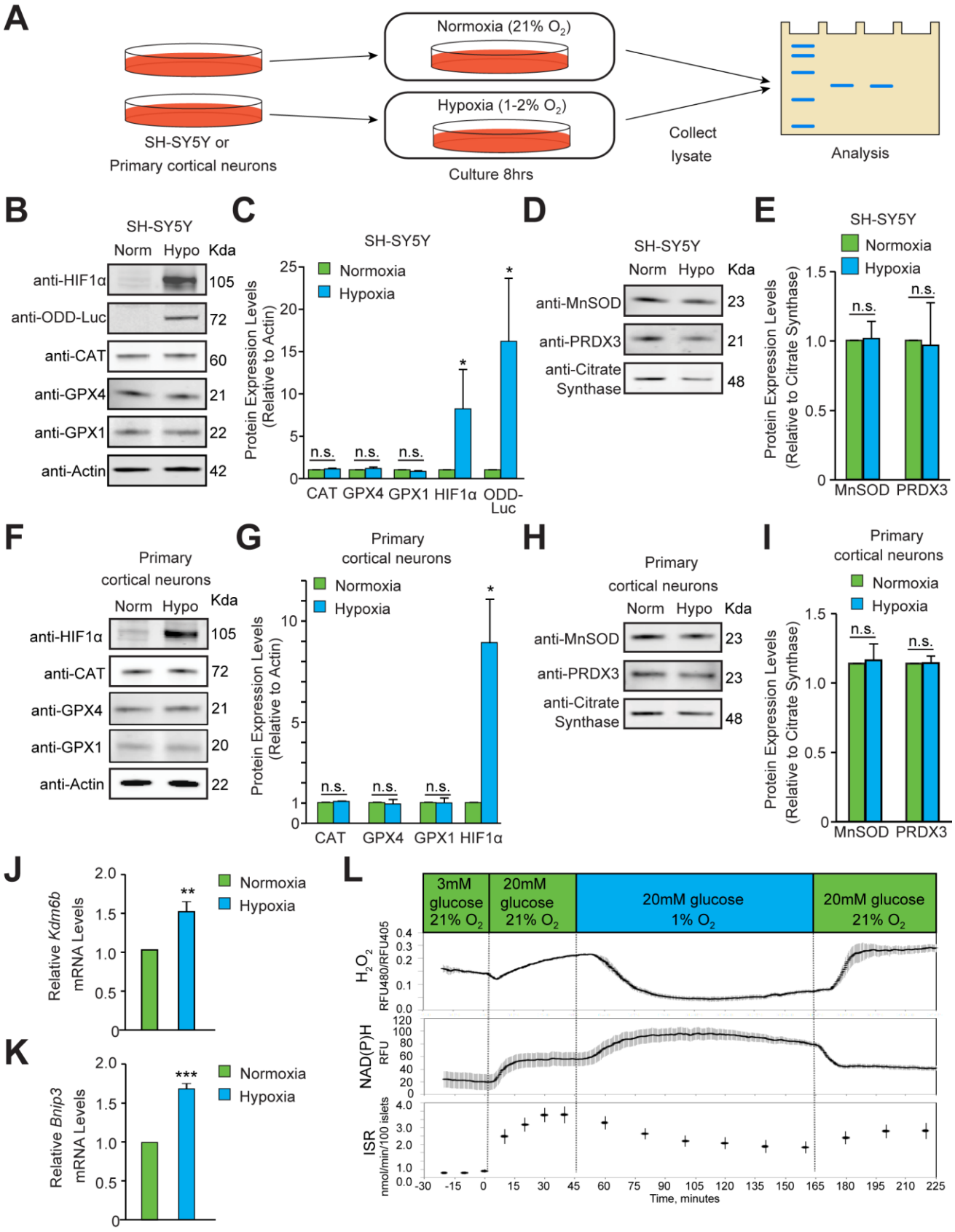
A
Normoxia (21% O2)
Hypoxia (1-2% O2)
SH-SY5Y or
Primary cortical neurons
Culture 8hrs
Collect
lysate
Analysis
B
SH-SY5Y
Norm Hypo Kda
anti-HIF1α 105
anti-ODD-Luc 72
anti-CAT 60
anti-GPX4 21
anti-GPX1 22
anti-Actin 42
C
SH-SY5Y
Normoxia
Hypoxia
Protein Expression Levels (Relative to Actin)
n.s.
CAT GPX4 GPX1 HIF1α ODD-Luc
D
SH-SY5Y
Norm Hypo Kda
anti-MnSOD 23
anti-PRDX3 21
anti-Citrate Synthase 48
E
SH-SY5Y
Normoxia
Hypoxia
Protein Expression Levels (Relative to Citrate Synthase)
n.s.
MnSOD PRDX3
F
Primary cortical neurons
Norm Hypo Kda
anti-HIF1α 105
anti-CAT 72
anti-GPX4 21
anti-GPX1 20
anti-Actin 22
G
Primary cortical neurons
Normoxia
Hypoxia
Protein Expression Levels (Relative to Actin)
n.s.
CAT GPX4 GPX1 HIF1α
H
Primary cortical neurons
Norm Hypo Kda
anti-MnSOD 23
anti-PRDX3 23
anti-Citrate Synthase 48
I
Primary cortical neurons
Normoxia
Hypoxia
Protein Expression Levels (Relative to Citrate Synthase)
n.s.
MnSOD PRDX3
J
Relative Kdm6b mRNA Levels
Normoxia
Hypoxia
K
Relative Bnip3 mRNA Levels
Normoxia
Hypoxia
L
3mM glucose 21% O2
20mM glucose 21% O2
20mM glucose 1% O2
20mM glucose 21% O2
H2O2 RFU480/RFU405
NAD(P)H RFU
ISR nmol/min/100 islets
Time, minutes

Figure 1. Hypoxia did not induce homeostatic increases in antioxidant enzymes or increase peroxide levels (A) Experimental approach employed to examine changes in the protein levels of endogenous antioxidant enzymes in hypoxia. **(B-I)** Immunoblots of catalase (peroxisome), GPX1 and GPX4 (cytosol and mitochondria) or MnSOD and PRDX3 (mitochondria) in **(B-E)** SH-SY5Y ODD Luc. cells that stably overexpressed ODD (HIF **O**xygen **D**ependent **D**omain-luciferase fusion) or **(F-I)** PCNs exposed to normoxia or hypoxia for 8h. The protein levels of catalase, GPX4, and GPX1 were normalized to actin while those of MnSOD and PRDX3 were normalized to the mitochondrial protein, citrate synthase. A monoclonal antibody to luciferase (indicated as anti-ODD-Luc. in the figure) was used to detect changes in ODD-luciferase protein levels in SH-SY5Y ODD-Luc. cells. **(J-K)** Pancreatic islets were exposed to hypoxia for 2h and then were lysed and processed for mRNA expression analysis of HIF1α target genes, *Kdm6b* and *Bnip3*. The densitometric data and gene expression data were pooled from three independent experiments in the form of mean ± SD. The statistical analyses of densitometric data and gene expression data were done using Student's t test (B-K). (n.s.) indicates non-significant difference, (**) indicates $p<0.01$ and (***) indicates $p<0.001$ with respect to respective normoxia controls. **(L)** Hypoxia leads to large decrease in H_2O_2 levels (top), increased NAD(P)H (middle), and decreased insulin secretion (bottom). Glucose stimulation by 20 mM glucose was added as reference, and oxygen levels were changed using an artificial gas equilibration device placed inline in the flow system. All three experiments were carried out separately, but using the same flow culture system.

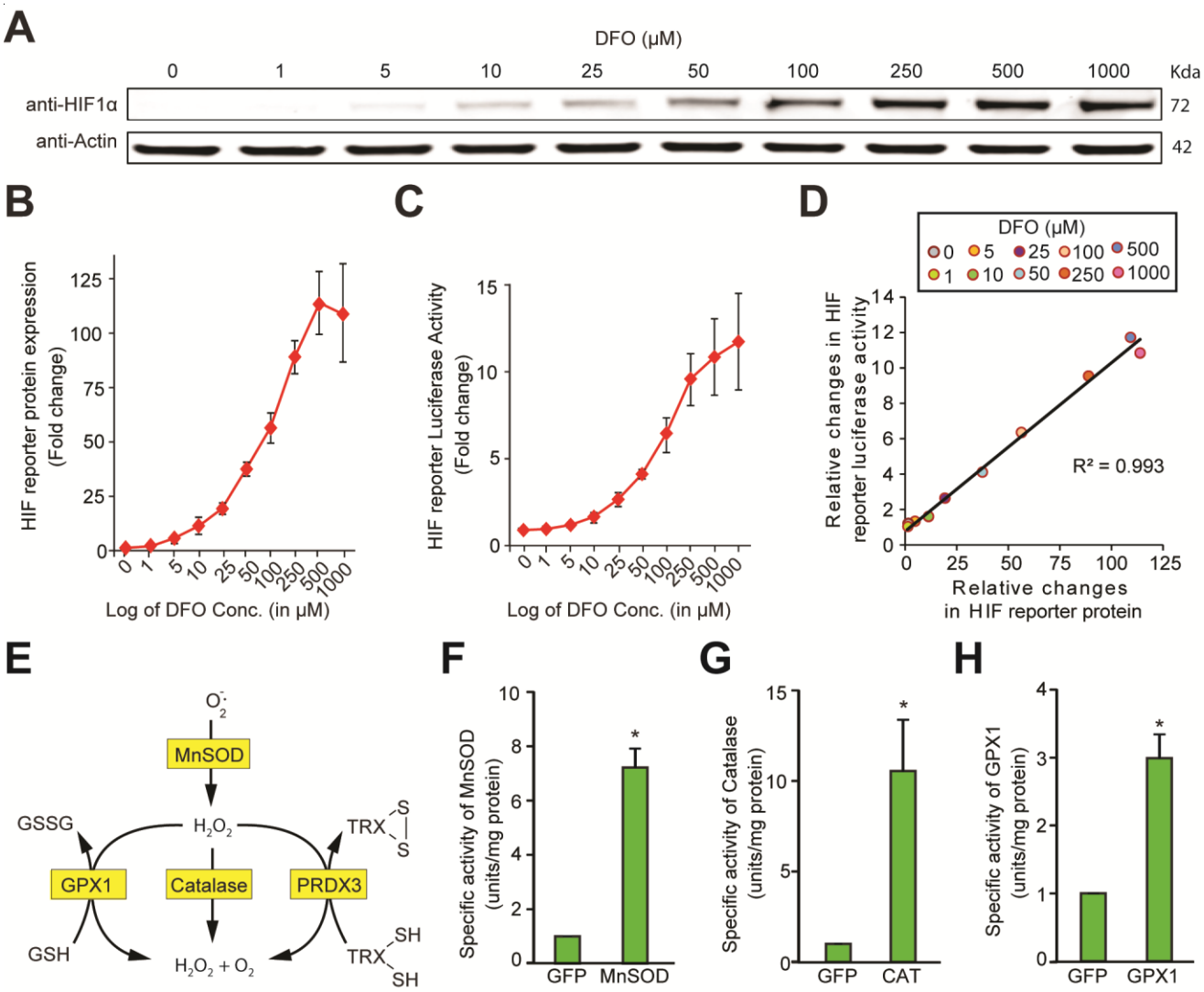

Figure 2. Validation of the sensitivity and the dynamic range of HIF1α protein and antioxidant enzyme activity measurements (A, B, C) SH-SY5Y ODD-Luc. cells were treated with increasing concentrations of DFO (1 μM-1 mM) for 3 h and were, thereafter, processed for assessment of either changes in HIF reporter protein (i.e. ODD-Luc. protein) level via immunoblotting **(A, B)** or changes in HIF reporter luciferase activity (i.e. ODD-luciferase activity) with luminometry. **(C)**. **(D)** Correlation between relative changes in HIF reporter luciferase activity (i.e. ODD-luciferase activity) and relative changes in HIF reporter protein (i.e. ODD-Luc. protein). **(E)** A schematic diagram showing known mechanisms of H_2O_2 detoxification by peroxisomal, cytosolic and mitochondrial antioxidants**. (F, G, H)** SH-SY5Y cells were transduced with adenoviral constructs encoding MnSOD, catalase, GPX1 or a GFP control and incubated for 72h for steady-state expression. Cells were processed for measurement of specific activities of these enzymes. Data were pooled from three independent experiments in the form of mean ± SD. The statistical analyses were performed using Student's t test. (*) indicates statistical difference of $p<0.05$ with respect to respective GFP control. "N" stands for normoxia and "H" stands for hypoxia.

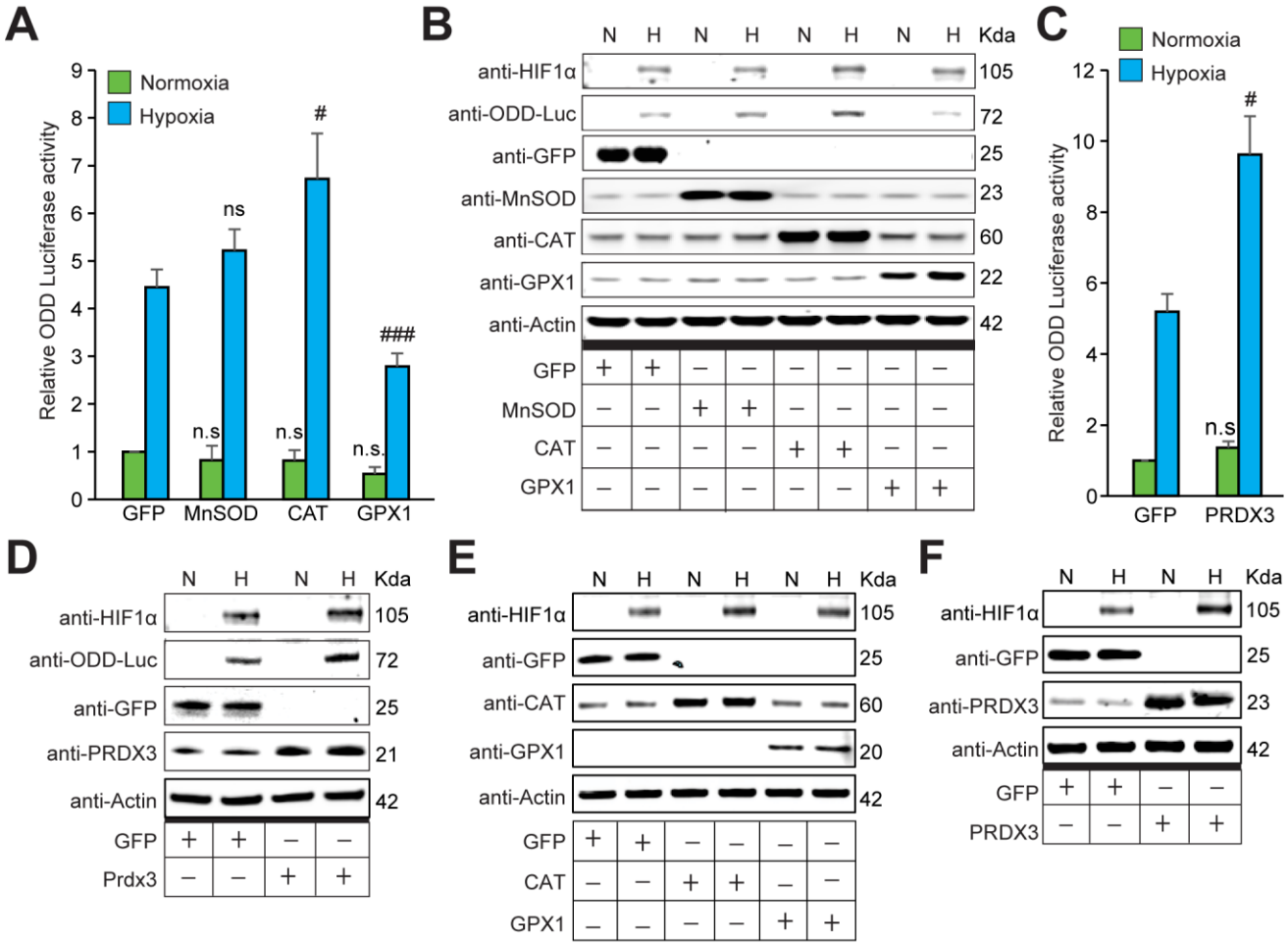

Figure 3. The stabilization of HIF1α is not oxidant-initiated in hypoxia (A, B, C, D) SH-SY5Y cells stably expressing ODD-luciferase were transduced with adenoviruses encoding distinct antioxidant enzymes for 72h and then exposed to normoxia or hypoxia in parallel and were either processed for luciferase activity assay (A measure of quantitative changes in ODD) **(A, B)** or immunoblot analysis (A measure of quantitative changes in protein levels of ODD and HIF1α) **(C, D)**. **(E, F)** Mouse primary neurons were transduced with adenoviral vectors encoding distinct antioxidant enzymes or GFP for 48h and then exposed to normoxia or hypoxia in parallel for 4h. Two way ANOVA with Bonferroni post-test was used for all comparisons. (n.s.) indicates non-significant difference with respect to GFP control under normoxia while (ns), (#) and (###) indicate non-significant difference and the statistical differences of $p<0.05$, and $p<0.001$, respectively, with respect to GFP control in hypoxia. All Western blot experiments were performed as three independent sets and a representative blot of each was shown in the figure.

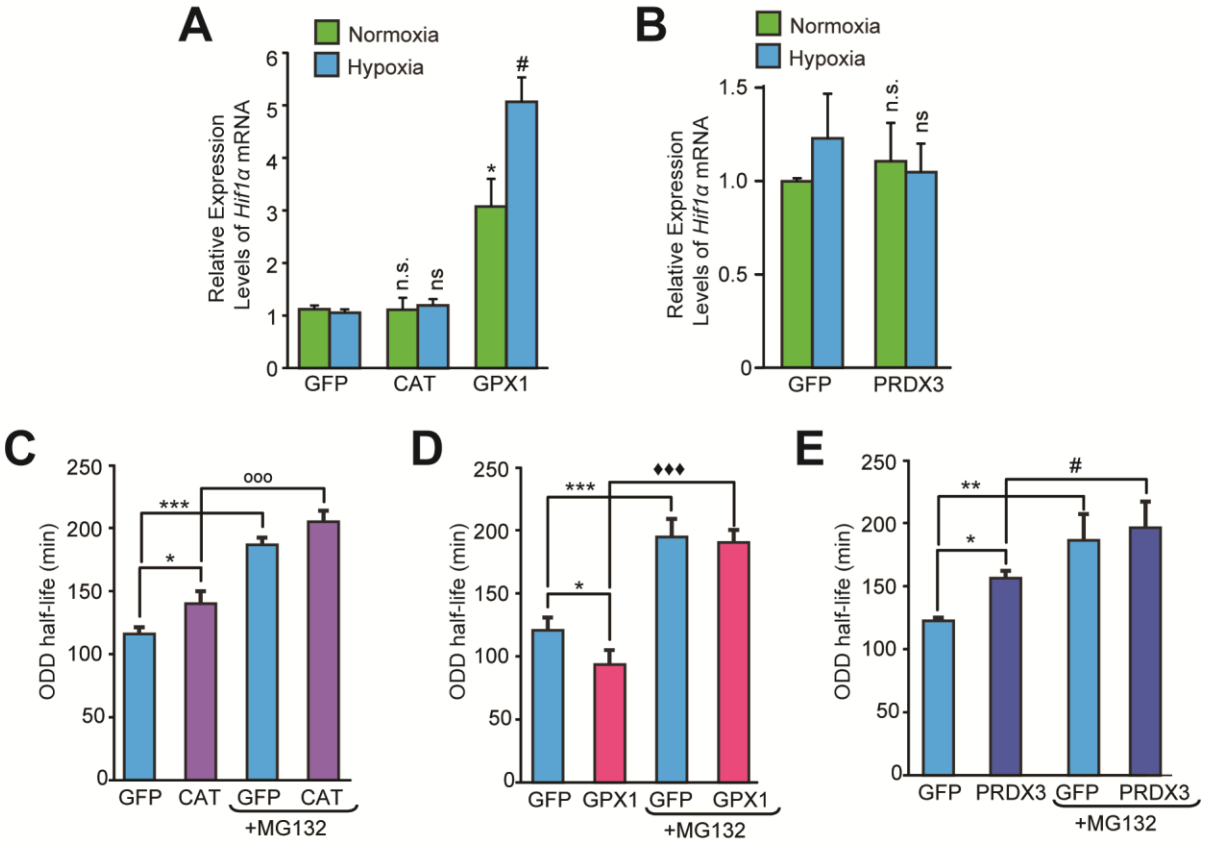

Figure 4. Divergent changes in HIF1α protein levels induced by antioxidant enzymes capable of scavenging peroxide cannot be attributed to differential changes in HIF1α mRNA synthesis or stability (A, B) Relative changes in *Hif1α* mRNA in SH-SY5Y cells in response to forced expression of various antioxidant enzymes. Data were pooled from three independent experiments in the form of mean ± SD. One way ANOVA with Dunnett's post-test was used for comparing cells expressing catalase or GPX1 with respect to cells expressing GFP and Student's t test was used for comparing cells expressing PRDX3 with respect to GFP. (n.s.) indicates non-significant difference with respect to respective GFP controls under normoxia while (ns) and (#) indicate non-significant difference and the statistical difference of $p<0.05$, respectively, with respect to GFP control in hypoxia. **(C, D, E)** Changes in half-life of HIF1α in SH-SY5Y ODD-Luc cells expressing catalase or GPX1 or PRDX3 with respect to that of respective GFP controls in hypoxia. ODD Half-life was assessed by performing a pulse chase experiment by adding 35µM cycloheximide at every twenty minutes for a total of four hours using luciferase activity assay in SH-SY5Y cells expressing these antioxidants pre-treated either with or without 10 µM MG132. Data were pooled from three independent experiments in the form of mean ± SD. Two way ANOVA with Bonferroni's post-test was used for statistical analysis. (*),

(**), and (***) indicate statistical differences of $p<0.05$, $p<0.01$ and $p<0.001$ with respect to respective GFP controls in hypoxia. (°°°), (♦♦♦) and (#) represent statistical differences of $p<0.001$ w.r.t CAT, $p<0.001$ w.r.t GPX1 and $p<0.05$ w.r.t PRDX3, respectively.

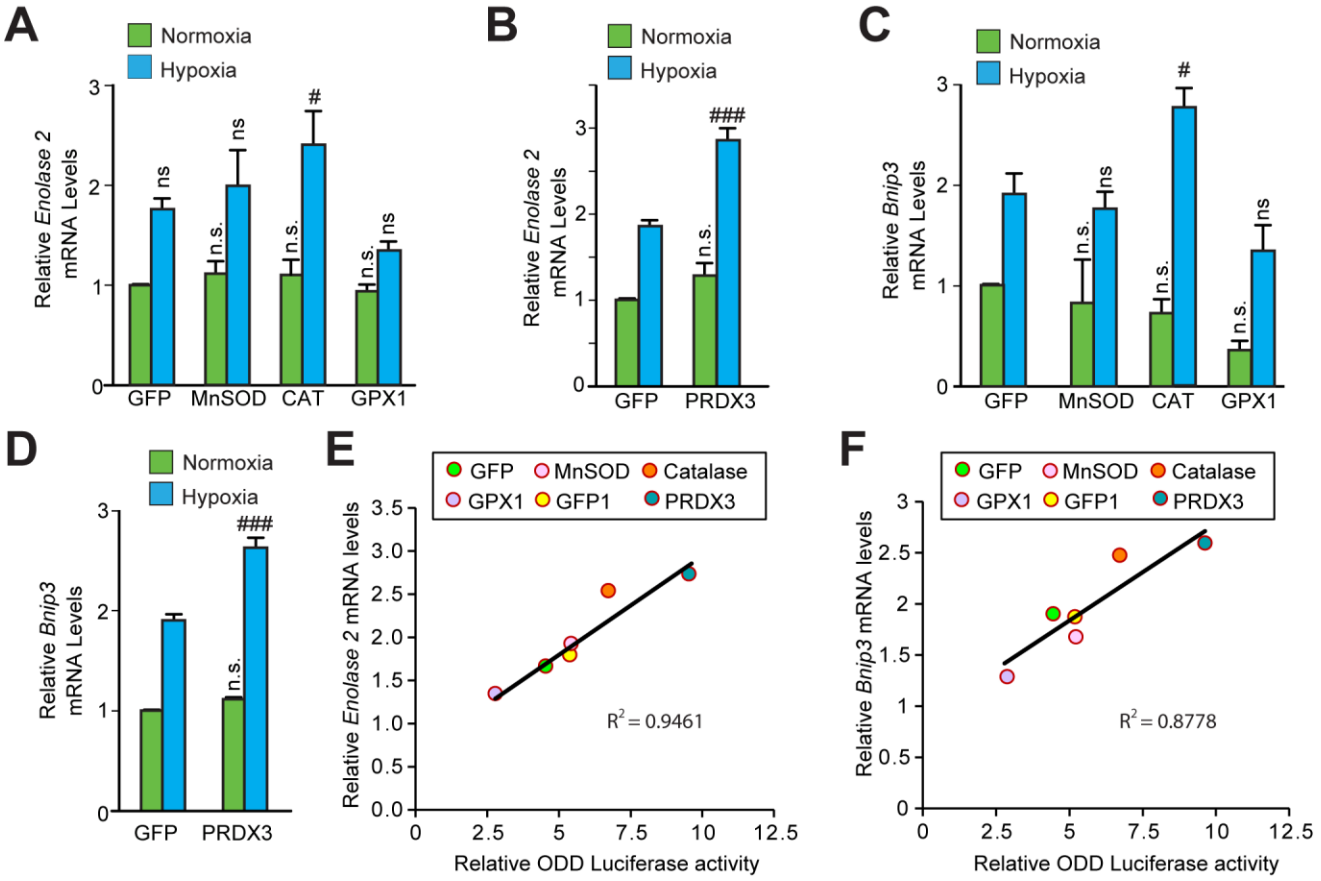

Figure 5. The transcriptional activity of HIF1α is not oxidant-initiated in hypoxia. Relative changes in mRNA levels of HIF1α target genes **(A, B)** *Enolase2* and **(C, D)** *Bnip3* in SH-SY5Y cells expressing various antioxidant enzymes as compared to that of respective GFP controls. Data were pooled from three independent experiments in the form of mean ± SD. One way ANOVA with Dunnett's post-test was used for comparing the statistical difference between cells expressing MnSOD, catalase or GPX1 with respect to that of GFP control and Student's t test was used to compare the statistical difference between cells expressing PRDX3 with that of GFP control. (n.s.) indicates non-significant difference with respect to respective GFP controls under normoxia only while (ns), (#) and (###) indicate non-significant difference, and the statistical differences of $p<0.05$, and $p<0.001$, respectively, with respect to GFP control in hypoxia. **(E, F)** Correlation between relative changes in either *Enolase2* or *Bnip3* and relative ODD-luciferase activities.

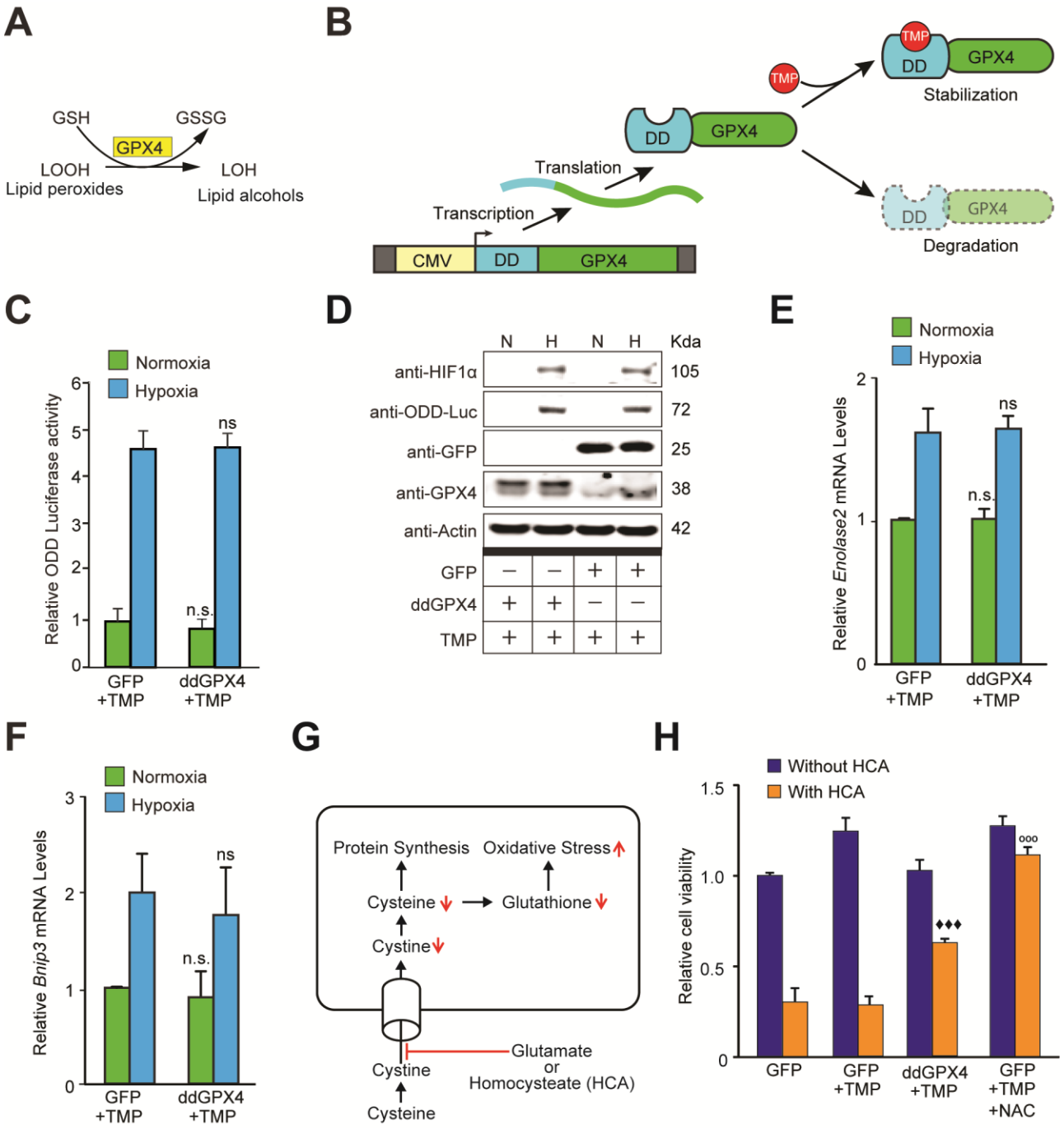

Figure 6. Reactive lipid species do not regulate HIF1α stabilization or its transcriptional activity in hypoxia (A) A schematic diagram showing that GPX4 converts lipid hydroperoxides into lipid alcohols using GSH as a cofactor. **(B)** A schematic showing regulated protein expression of GPX4 fusion containing an optimized destabilization domain when exposed to the antibiotic, Trimethoprim (TMP). Reversible stability of GPX4 protein was conferred by fusing its coding sequence to a destabilization domain sequence (mutants of *E. Coli* dihydrofolate reductase). Accordingly, GPX4 protein possessing the destabilization domain is degraded resulting in low steady levels of GPX4. Trimethoprim binds to and neutralizes the destabilization

domain stabilizing GPX4 protein in a dose dependent manner. **(C, D)** SH-SY5Y ODD-Luc cells were transduced with adenoviral vectors encoding a destabilized form of GPX4 (ddGPX4) or GFP and then exposed to normoxia/hypoxia and were either processed for luciferase activity assay (C) or immunoblotting (D). 10 µM TMP was added to ddGPX4 expressing cells after 60h of adenoviral incubation for 12h in order to achieve stabilized GPX4 expression. **(E, F)** Relative changes in mRNA levels of HIF1α target genes, *Enolase2* and *Bnip3* in SH-SY5Y cells. **(G)** A schematic diagram depicting the glutathione depletion model of oxidative stress. **(H)** PCNs were transduced with GFP/GPX4 for 24h and then treated with 5 mM HCA. Cells were simultaneously treated with 10 µM TMP. Then, cells were incubated for 24h to induce oxidative stress. Thereafter, viability of cells was measured via the MTT assay. 100 µM NAC was used as positive control. The final values were pooled as mean ± S.D. of three independent experiments. Two way ANOVA with Bonferroni's post-test was used for statistical analyses. One way ANOVA with Dunnett's post-test was used for comparing DCF fluorescence and viability. (n.s.), (*) and (***) indicate non-significant difference, and the statistical differences of $p<0.05$, and $p<0.001$, respectively, with respect to GFP control under normoxia while (ns), (#) and (###) indicate non-significant difference, and the statistical differences of $p<0.05$, and $p<0.001$, respectively, with respect to GFP control in hypoxia. (°°°) indicates statistical difference of $p<0.001$ with respect to GFP treated with HCA only while (♦♦♦) indicates statistical difference of $p<0.001$ with respect to GFP treated with both TMP and HCA.

.

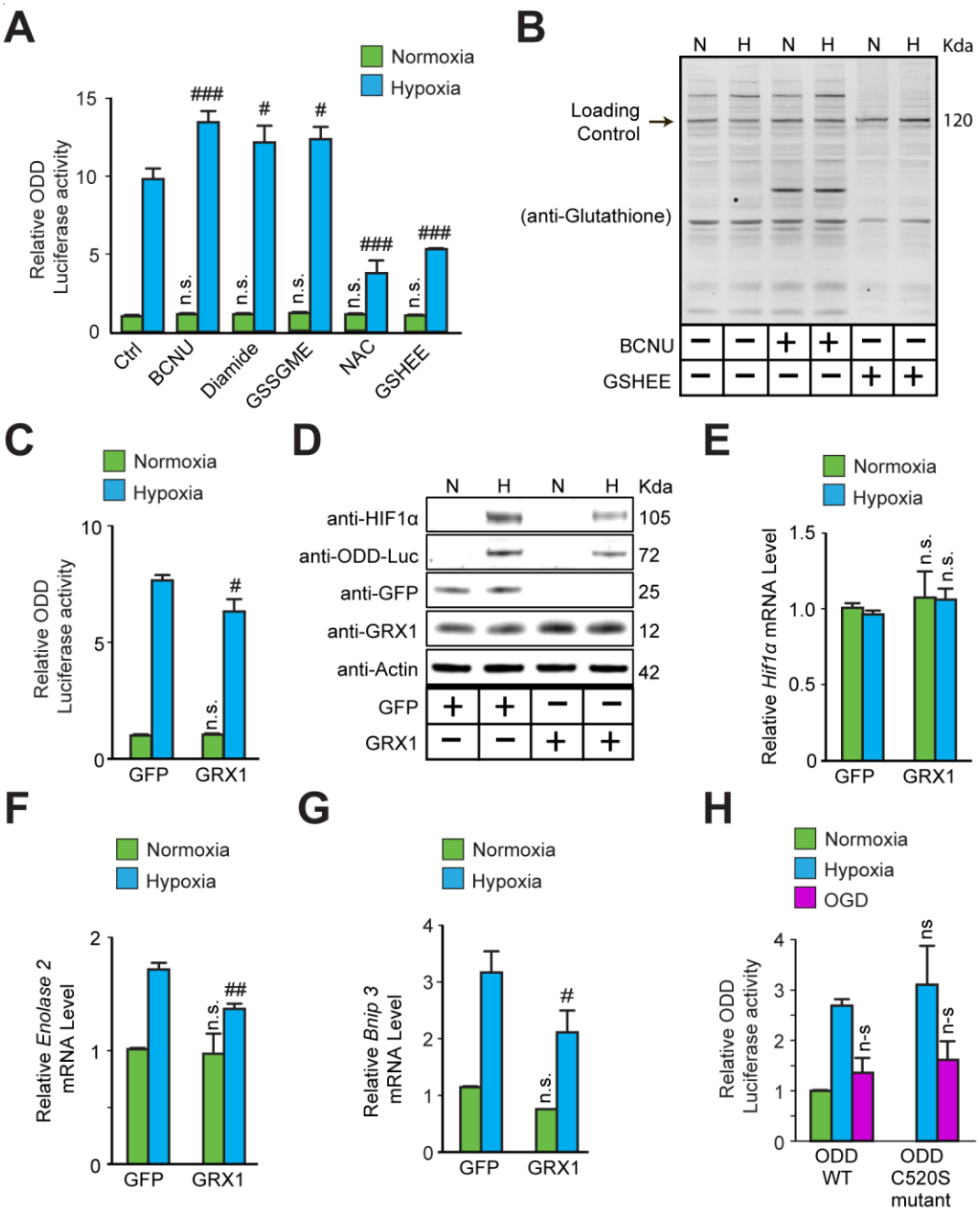

Figure 7. The stabilization and activity of HIF1α is tuned by the cellular redox state in hypoxia (A) SH-SY5Y ODD-Luc. cells were treated with either 20 µM BCNU, 100 µM diamide, 1 mM GSSG methyl ester (GSSGME), 10 mM NAC, or 1mM GSH ethyl ester (GSHEE), and incubated in normoxia/hypoxia in parallel for 4h followed by luciferase activity assessment. **(B)** Changes in global protein *S*-glutathionylation in response to 20 µM BCNU or 1 mM GSHEE treatment in normoxia/hypoxia for 4h. **(C)** SH-SY5Y ODD-Luc. cells were transduced with adenoviral vectors encoding GFP or GRX1 for 72h followed by luciferase activity assessment. **(D)** Immunoblots of ODD-luciferase and HIF1α proteins in cells expressing GFP or GRX1. **(E)** Relative change in *Hif1α* mRNA in SH-SY5Y cells expressing GRX1 compared to cells expressing GFP. **(F, G)** Relative changes in mRNA levels of *Enolase2* and *Bnip3* in SH-SY5Y

cells expressing GRX1 as compared to those expressing GFP. **(H)** Changes in ODD-luciferase activity in SH-SY5Y cells transiently transfected with a cDNA expressing ODD-luciferase or ODD C520S-luciferase for 24h and then exposed to either normoxia or hypoxia or oxygen-glucose deprivation (OGD) for 4h. The final values were pooled as mean ± S.D. of three independent experiments in all cases. Two way ANOVA with Bonferroni's post-test was used for statistical analyses. (n.s.) and (**) indicate non-significant difference, and the statistical difference of $p<0.001$, respectively, with respect to control under normoxia while (ns), (#), (##) and (###) indicate non-significant difference, and the statistical differences of $p<0.05$, $p<0.01$ and $p<0.001$, respectively, with respect to control in hypoxia. n-s indicate non-significant difference with respect to control under OGD.

A

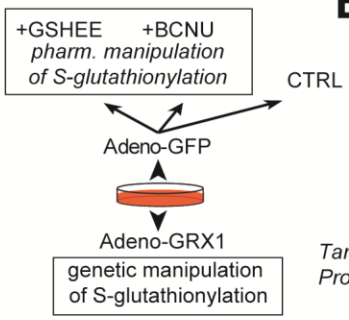

B

		Relative S-Glutathionylaion Levels							
	Culture Condition	Normoxia				Hypoxia			
	Treatment Condition	GRX1	GSHEE	BCNU	BCNU	GRX1	GSHEE	BCNU	BCNU
	S-Glutathionylation Levels Normalized to	CTRL	CTRL	CTRL	GSHEE	CTRL	CTRL	CTRL	GSHEE
Target Protein	PHD1 / PHD2 / PHD3 / HIF1α / VHL / SIAH	ND	ND	ND	ND	ND	ND	ND	ND

C

	Relative S-Glutathionylaion Levels								
	Normoxia				Hypoxia				Culture Condition
	GRX1	GSHEE	BCNU	BCNU	GRX1	GSHEE	BCNU	BCNU	Treatment Condition
Target Protein	CTRL	CTRL	CTRL	GSHEE	CTRL	CTRL	CTRL	GSHEE	S-Glutathionylation Levels Normalized to
RPN1	0.598 p≤0.26	0.659 p≤0.38	0.623 p≤0.38	0.89 p≤0.9	0.358 p≤0.05	0.586 p≤0.26	1.684 p≤0.26	3.849 p≤0.001	
RPN2	0.635 p≤0.32	0.44 p≤0.05	0.328 p≤0.05	0.86 p≤0.8	0.685 p≤0.6	0.91 p≤0.98	100 p≤0.0001	100 p≤0.0001	

Dec. Relative S-Glutathionylaion Levels Inc.

D

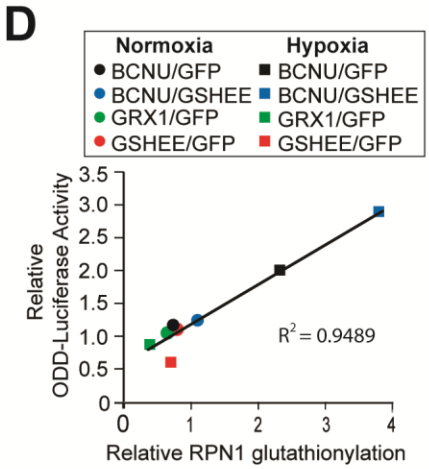

E

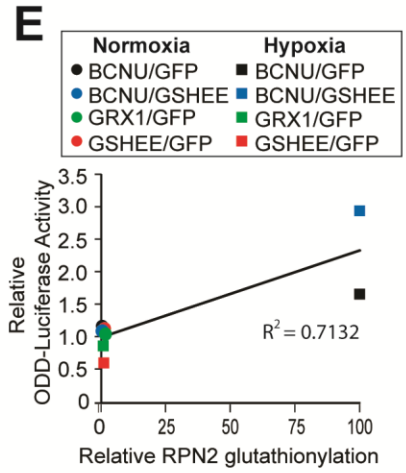

F

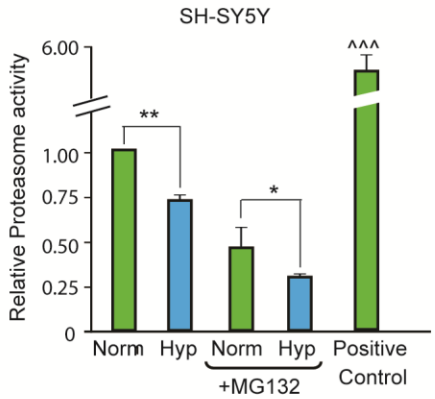

G

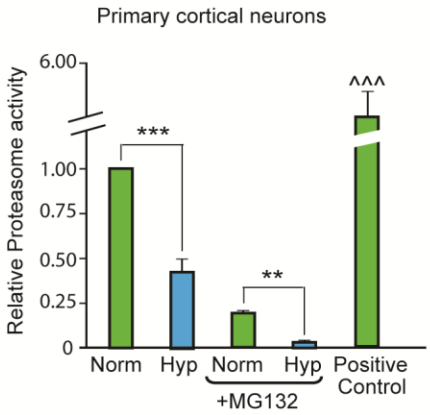

H

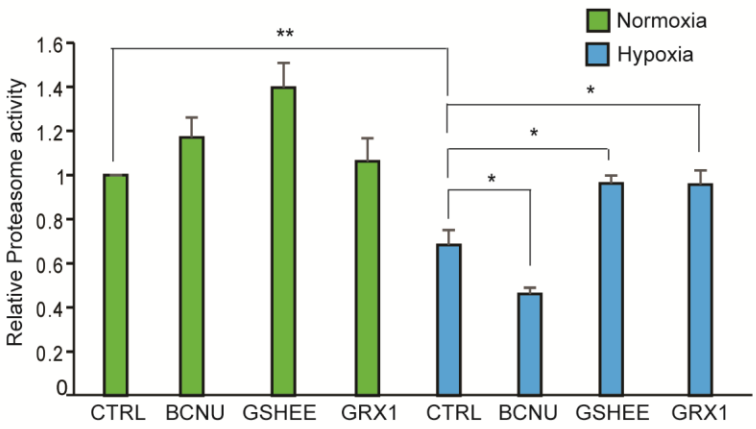

Figure 8. Non-targeted proteomic analysis of *S*-glutathionylated proteins in hypoxia shows that hypoxia-specific regulators of HIF1α stability are not regulated by redox modulation. Unexpectedly, Rpn1 and Rpn2, subunits of the proteasome are significantly *S*-glutathionylated (A) A schematic diagram of the experimental paradigm used to analyze the *S*-glutathionylated proteome in normoxia and hypoxia using agents known to modulate the cellular redox state. SH-SH5Y cells were transduced with adenoviral vectors encoding GFP or GRX1 for 72hours. Thereafter, cells expressing GFP were treated with either BCNU (20 µM) or GSHEE (1 mM) or untreated (working as control) and were simultaneously exposed to normoxia/hypoxia for 4h followed by their lysis and proteomics analysis for *S*-glutathionylated proteins. **(B)** *S*-glutathionylation of regulators of HIF1α stability were not detected (N.D.) in the proteomics analysis. **(C)** Changes in *S*-glutathionylation of the proteasomal regulatory subunits, Rpn1 and Rpn2 from the proteomics analysis. $p < 0.05$ equals statistical significance. **(D, E)** Correlation between relative changes in the stability of HIF-1 reporter (ODD-luciferase activity) and relative changes in the *S*-glutathionylation of Rpn1 and Rpn2 under reducing or oxidizing conditions. **(F, G)** Proteasomal activities of SH-SY5Y cells and PCNs exposed to normoxia/hypoxia for 4h in the presence/absence of proteasomal inhibitor, MG132 (10µM). One way ANOVA with Tukey's post-test was used to compare the statistical differences between samples. (*), (**) and (***) indicate statistical differences of $p<0.05$, $p<0.01$ and $p<0.001$ with respective comparisons. Student's t test was used to compare the positive control provided in the kit with normoxia control. (^^^) represents statistical differences of $p<0.001$ with respect to normoxia control. **(H)** Proteasomal activities of SH-SY5Y cells treated as described above in (A). One way ANOVA with Tukey's post-test was used to compare the statistical differences between samples. (*) and (**) indicate statistical differences of $p<0.05$ and $p<0.01$ with respective comparisons.

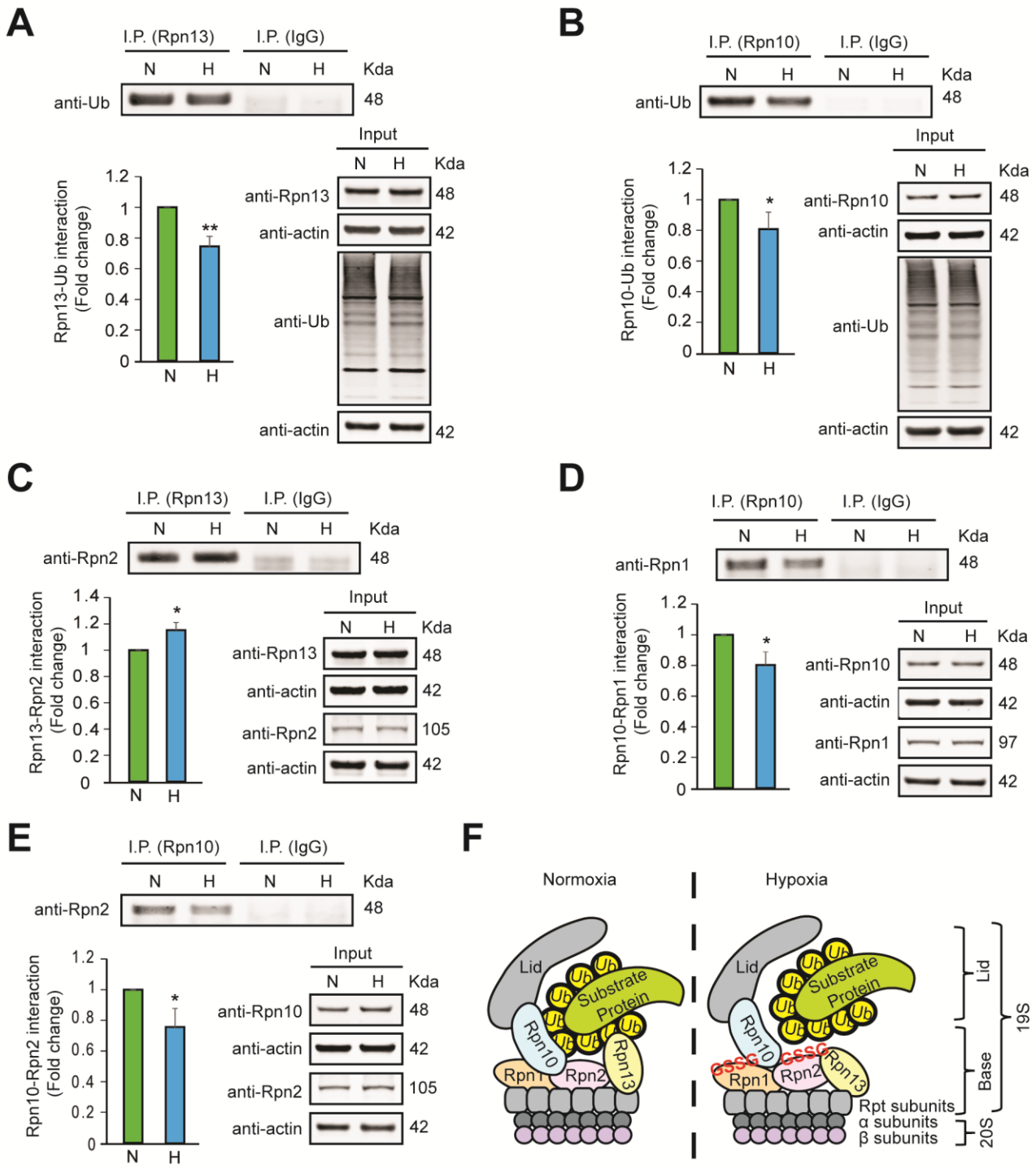

Figure 9. Hypoxia diminishes the interaction of ubiquitinated substrates with ubiquitin receptors, Rpn13 and Rpn10. All immunoprecipitations were performed in SH-SY5Y cells treated with MG132 (10 µM) followed by their exposure to normoxia or hypoxia for 4h in parallel (A-E). **(A)** Immunoprecipitation of Rpn13 with Ubiquitin (Ub) **(B)** Immunoprecipitation of Rpn10 with Ubiquitin **(C)** Immunoprecipitation of Rpn13 with Rpn2 **(D)** Immunoprecipitation of Rpn10 with Rpn1 **(E)** Immunoprecipitation of Rpn10 with Rpn2 **(F)** A schematic diagram demonstrating

hypoxia led changes in interactions of various Rpn subunits present in the 19S regulatory cap of the proteasome among themselves and also in interactions of ubiquitin receptors, Rpn10 and Rpn13 with polyubiquitinated substrates. All immunoprecipitation experiments were performed as three independent sets and a representative blot of each has been shown in the figure. The densitometric analyses of three independent sets of each I.P. blots has been represented as bar diagram along with each immunoprecipitation blot. Student's t test was used to compare the statistical difference between respective protein interactions in normoxia and hypoxia. (*) and (**) indicate statistical differences of $p<0.05$ and $p<0.01$, respectively, with respect to normoxia.